De transnationale Universiteit Limburg is een uniek samenwerkingsverband van twee universiteiten in twee landen:
de Universiteit Hasselt en Maastricht University

universiteit hasselt
UNIVERSITEIT VAN DE TOEKOMST

Maastricht University

Universiteit Hasselt | Campus Diepenbeek | Agoralaan Gebouw D | BE-3590 Diepenbeek
Universiteit Hasselt | Campus Hasselt | Martelarenlaan 42 | BE-3500 Hasselt

GENEESKUNDE

master in de biomedische wetenschappen: bio-elektronica en nanotechnologie

2010
2011

Masterproef

Cubic Boron Nitride Thin Films as Alternative Platform for Biosensor Applications

Promotor :
Prof. dr. Hans-Gerhard BOYEN

Copromotor :
Prof. dr. Patrick WAGNER

Fabian Wilbers

Masterproef voorgedragen tot het bekomen van de graad van master in de biomedische wetenschappen , afstudeerrichting bio-elektronica en nanotechnologie

Maastricht University

universiteit hasselt
UNIVERSITEIT VAN DE TOEKOMST

2010
2011

GENEESKUNDE

master in de biomedische wetenschappen: bio-elektronica en nanotechnologie

Masterproef

Cubic Boron Nitride Thin Films as Alternative Platform for Biosensor Applications

Promotor :
Prof. dr. Hans-Gerhard BOYEN

Copromotor :
Prof. dr. Patrick WAGNER

Fabian Wilbers

Masterproef voorgedragen tot het bekomen van de graad van master in de biomedische wetenschappen , afstudeerrichting bio-elektronica en nanotechnologie

Maastricht University

universiteit hasselt
UNIVERSITEIT VAN DE TOEKOMST

Contents

List of Figures

List of Abbreviations

a-BN	amorphous Boron Nitride
AFM	Atomic Force Microscope
c-BN	cubic Boron Nitride
DI	deionized
DNA	Deoxyribonucleic acid
EDC	1-Ethyl-3-(3-dimethylaminopropyl)carbodiimide
FTIR	Fourier Transformed Infrared Spectroscopy
FWHM	Full Width at Half Maximum
GATR	Grazing Angle Attenuated Total Reflection
h-BN	hexagonal Boron Nitride
MES	2-(N-morpholino)ethanesulfonic acid
NCD	nanocrystalline diamond
PECVD	Plasma Enhanced Chemical Vapor Deposition
r-BN	rhombohedral Boron Nitride
r.f.	radio frequency
SDS	Sodium Dodecyl Sulfate
SFE	Surface Free Energy
SSC	Saline-sodium citrate
ssDNA	single stranded DNA
t-BN	turbostratic Boron Nitride
UHV	Ultra High Vacuum
w-BN	wurtzite Boron Nitride
XPS	X-ray Photoelectron Spectroscopy

Abstract

The wide band gap material cubic Boron Nitride (c-BN) as functional substrate in biosensor applications has the extraordinary potential to serve as novel biosensor platform. Besides its structural and electronic similarities to the widely used nanocrystalline diamond (NCD) thin films, c-BN exhibits a set of properties which could make it even superior for biosensor applications. As c-BN is a compound synthesized by equal amounts of boron and nitrogen atoms, corresponding thin films reveal strong dipolar moments (due to ionic contributions to the B–N bonds) as well as new binding sites for functionalization. Boron and nitrogen at the sample surface offer new possibilities for binding target molecules and provide new functional groups that might allow direct binding of specific molecules as recognition elements for biosensor applications.

This work focusses on the preparation of high quality c-BN thin films by means of radio frequency (r.f.) magnetron sputtering under Ultra High Vacuum (UHV) conditions and the exploration of new routes for the functionalization of these surfaces. For this purpose, well-established functionalization protocols with 10-undecanoic acid (Fatty Acid) under UV light as well as new protocols for c-BN with linker molecules such as Diazonium were investigated. In addition, the feasibility to directly couple carboxyl-terminated single stranded DNA (ssDNA) to amine groups at the Boron Nitride surface was investigated.

For analysis, both surface sensitive techniques such as X-ray Photoelectron Spectroscopy (XPS), Atomic Force Microscope (AFM) and Contact Angle measurements, but also bulk sensitive techniques like Fourier Transformed Infrared Spectroscopy (FTIR) were performed. The DNA coverage on the substrates was investigated with the help of Confocal Fluorescence Microscopy.

It is found, that high quality c-BN with cubic phase contents higher than 70 % can be functionalized with both Fatty Acid and Diazonium. Surface coverages of DNA linked to the surface via both types of linker molecules were in the range of 8×10^{12} cm^{-2}. Direct coupling of carboxyl-terminated ssDNA did not show covalent linkage.

1 Introduction

This work focusses on the investigation of cubic Boron Nitride (c-BN) as a new platform for biosensor applications. The preparation of high quality c-BN and its feasibility to serve as permanent binding site for the recognition layer of a biosensor were investigated.

Sensors in general are devices capable of monitoring and detecting physical, chemical or biological properties and transducing these properties into electrical signals that can be analyzed. To achieve this, only target molecules from the analyte pass the sensor's preselection filter. A sensor platform is covered with a recognition layer that specifically reacts with the target molecules. At this recognition layer the target molecules undergo a physical, chemical or biological process which leads to a detectable event for the transducer unit. The transducer unit renders the event into a measurable signal such as voltage, current, impedance or others. An electrical interfaces serves for amplification and noise reduction of the signal induced by the transducer unit. The user interface of the sensor allows data interpretation and storage by the user. The setup of a general sensor as described in literature[1] is shown in Figure 1.1.

In contrast to other sensors, biosensors possess a recognition layer consisting of elements from biological origin. In the case of this work, these

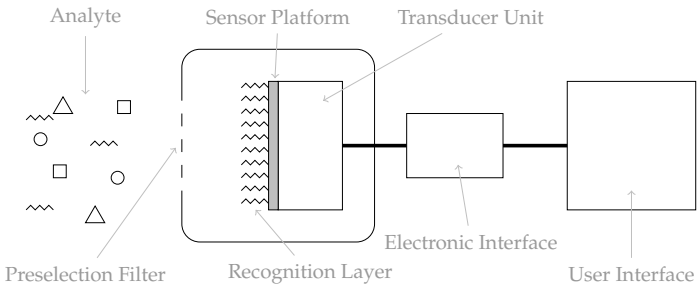

Figure 1.1: General setup of a sensor: Target molecules from the Analyte pass a Preselection Filter and form an event at the Recognition Layer. The Transducer Unit renders this event into a signal that can be amplified by the Electronic Interface and analyzed and stored by the User Interface.

recognition elements are single stranded DNA (ssDNA) molecules which allow hybridization with the complementary ssDNA string as target molecule. Impedance spectroscopy can be used to identify mismatches between target from the patient and recognition DNA at the recognition layer of the biosensor. This way, point mutations on patient's DNA can be detected in an easy and fast manner[2].

Special attention for biosensors lies within the sensor platform and the recognition layer. It is crucial to ensure that the recognition layer is covalently bond to the sensor platform in order to provide reusability of the biosensor and to avoid misinterpretation of the acquired signals due to changes induced by degradation of the recognition layer.

Currently, state-of-the-art biosensors use a diamond based platform where nanocrystalline diamond (NCD) thin films serve as platform for the transducer unit due to their chemical inertness against body fluids, their well established deposition methods, handling and procedures for functionalization[3]. Diamond and c-BN are similar in many characteristics, such as their analogous phases, high hardness, thermal conductivity and further properties, as will be explained in the following chapters. However, the main difference between NCD and c-BN in regard to functionalization properties lies with the fact that c-BN composes of two different types of atoms: Boron and nitrogen. Due to the differences of these two atoms in in electronegativity, the surfaces of c-BN possess dipolar moments that give rise to an induced ionic character. This can have advantages for the functionalization with DNA, since DNA itself is a slightly negative charged molecule.

The presence of boron and nitrogen at the c-BN sample surface opens a wide range of functionalization possibilities and might allow direct coupling of carboxyl-terminalized molecules with the help of the EDC-protocol.

The main reason why c-BN is not widely used in practice is that it is a purely synthetic material which has shown difficulties to produce in stable quality. Thin films tend to delaminate from silicon substrates and are unstable in aqueous conditions. Depositing c-BN on NCD substrates, as performed for this work, has shown that the internal stress could be drastically reduced[4] and that stable films, in aqueous solutions even stable for longer time periods, could be produced.

In this work, high quality c-BN thin films were produced by means of r.f. magnetron sputtering. In order to investigate the applications of c-BN

as biosensor platform, three different approaches for the functionalization of these thin films were studied.

The first approach focusses on 10-undecanoic acid (Fatty Acid) as linker molecule. The well established Fatty Acid linker used for the functionalization of diamond surfaces for sensing applications was adopted. It has previously been shown that this approach works for c-BN surfaces [5].

In a second approach, the Diazonium protocol was taken into account. This has proven to work well on diamond surfaces and in this work is being adjusted and investigated for its use with c-BN.

The final approach focuses on a set of experiments to investigated whether carboxyl functionalized DNA can be coupled to c-BN without a linker molecule by means of EDC mediated coupling, using the amine groups present at the surface of c-BN.

2 Materials & Methods

Boron Nitride is a purely synthetic material which is isostructural and isoelectrical to diamond due to similar crystal structures since boron and nitrogen are positioned next to carbon in the periodic table of elements. Cubic Boron Nitride cubic Boron Nitride (c-BN)) exhibits the second highest hardness next to diamond, a very high thermal conductivity, low thermal expansion and a low dielectric constant. It is a semiconductor, its band gap of 6.3 eV is higher that that of diamond with 5.5 eV. In contrast to diamond, c-BN can be doped both n- and p-type. It is chemically inert against molten ferrous materials and it has been reported, that c-BN is inert against oxygen[6]. In addition it has shown a high transmittance over a wide range of the optical spectrum.

The B–N atomic distance is 1.57 Åand c-BN has a density of 3.48 g/cm^3. Besides the covalent stability, the bond shows dipole moments and an induced ionic character due to the differences in electronegativity of boron and nitrogen. This allows not only to investigate c-BN with Fourier Transformed Infrared Spectroscopy (FTIR), but also holds advantages in regard to functionalization since the surface has a polar character unlike diamond.

Similar to carbon, Boron Nitride exists in different analogous phases including cubic Boron Nitride (c-BN), hexagonal Boron Nitride (h-BN), wurtzite Boron Nitride (w-BN), rhombohedral Boron Nitride (r-BN), amorphous Boron Nitride (a-BN) and turbostratic Boron Nitride (t-BN).

The cubic form is the most advantageous and has a zinc blende lattice structure with sp^3 hybridized B–N σ-bonds (see Figure 2.1). It is similar to the cubic diamond structure. The wurtzitic structure is bonded by sp^3 bonds as well, but the angles between the tetrahedron of boron and nitrogen atoms are different. The hexagonal form of Boron Nitride is a soft, graphite like layered compound with stacked hexagonal rings of basal planes rotated by 180° in every plane. The in plane atoms are sp^2 hybridized, the out of plane atoms are bond by weak π orbitals. The rhombic crystal structure of boron nitride is sp^2 hybridized and basal planes are stacked but only three B–N bonds in the out of plane direction share π orbitals. Both amorphous and turbostratic are disordered struc-

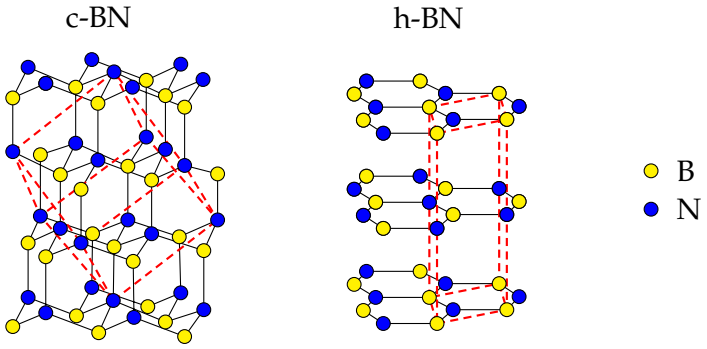

Figure 2.1: Cubic and hexagonal structure of Boron Nitride

tures, in t-BN the hexagonal basal planes are stacked in random sequence and with random rotations about the c-axis.

In contrast to diamond, c-BN films are not as prominent in surface functionalization. This may come from the fact that although c-BN has been reported in 1957 for the first time[7] there are still difficulties in synthesizing high quality films. Thin films grown on silicon induce high stress in the films which is caused by the large lattice mismatch between c-BN and Si[6]. It has also been reported that prior to c-BN growth, a h-BN[8] or a-BN/t-BN[9] intermediate layer grows. In combination with the stress of the thin film, this leads to easily delaminating thin films that become unstable the thicker the film grows. Since the stability of a biosensor platform is crucial and needs to be stable even in aqueous solutions for long time periods, c-BN thin films are grown with an intermediate layer of nanocrystalline diamond (NCD). This way, the lattice mismatch and the stress is reduced drastically and the stability of the film is increased as the h-BN interlayer between NCD and c-BN is reduced[10].

On top of any c-BN thin film, a thin hexagonal-like layer is deposited. It has been reported, that this layer has a thickness of about 0.9 nm[11]. This layer can be removed with the help of a microwave hydrogen plasma, as described in chapter 3.

2.1 Substrate preparation

As primary substrate 3″ double side polished Si(100) wafers were used, unless mentioned differently in the text. All samples in all states of procedure were stored in a glass exsiccator at low pressure to reduce contamination by (dust-) particles and to minimize the influence by air and water.

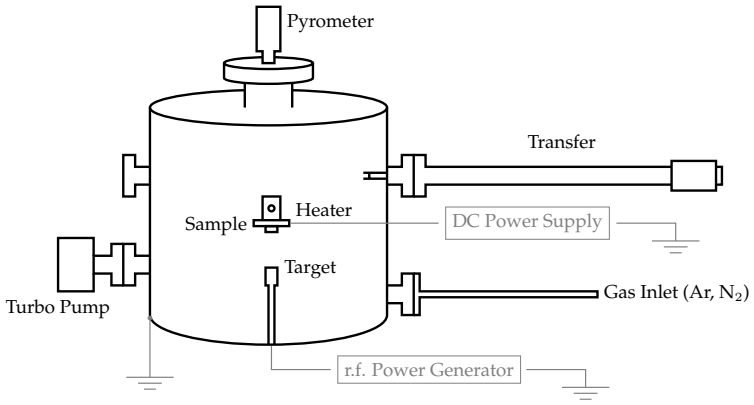

Figure 2.2: c-BN deposition chamber: The sample can be rotated, facing to the pyrometer, transfer or target thus allowing different sample treatments and procedures to be carried out and monitored.

NCD thin films

NCD thin films were prepared by the diamond group of IMO with the help of Plasma Enhanced Chemical Vapor Deposition (PECVD)[2]. The primary substrate wafer of Si(100) was cleaned through the RCA standard wafer cleaning procedure[12] prior to diamond film growth. A gas mixture of 460 sccm H_2 and 40 sccm CH_4 (8 %) yielded a total gas pressure of 22 torr (29 mbar) during growth. The microwave plasma with a power of 3000 W at a temperature of 500°C for 2 h 45 min resulted in a film thickness of approximately 100 nm. The 3″ wafer was cut into 5 x 10 mm samples for further film growth in the c-BN deposition chamber.

c-BN thin films

c-BN thin films were prepared using the 5 x 10 mm Si(100) substrates with a thin film of NCD. The deposition of c-BN was performed using radio frequency (r.f.)-magnetron sputtering with a sample-to-target distance of 30 mm and a plasma power of 65 W at a temperature of 700–800 °C. The target was pure h-BN and for cleaning it was pre-sputtered for a time period of 3 minutes before deposition. At a base pressure in the range of 1.0×10^{-7} mbar argon and nitrogen gas were introduced for deposition to the chamber at 100 sccm respectively, resulting in a working pressure of 7×10^{-2} mbar. Deposition time of 40 min and the applied bias voltage for deposition of -220 V resulted in film thickness of 80-100 nm. A schematic overview of the deposition chamber is given in Figure 2.2.

After deposition, c-BN films were hydrogenated in an ex situ H_2 microwave plasma of 3500 W at a working pressure of 30 torr (40 mbar) and 600 °C for two minutes.

2.2 Surface functionalization

All the prepared c-BN surfaces, regardless of their linker molecule, were functionalized using 1-Ethyl-3-(3-dimethylaminopropyl)carbodiimide (EDC).

EDC is a widely used carbodiimide which acts as an activating agent for the coupling of carboxyl groups to primary amines. By nucleophilic substitution, a stable amine bond is created. The chemical equation for this is shown in Figure 2.3. For this study, all samples have been activated using the EDC-protocol[13].

The Deoxyribonucleic acid (DNA) used for attachment was 8 base pair ssDNA, synthetically produced by EUROGENTECH. For Fatty Acid and Diazonium linkage, amino-terminalized ssDNA was used. The functional group is bound to the 5′ end of DNA with a C_6H_{12}-spacer. The base sequence and chemical formula are: NH_2–C_6H_{12}–CCC CTG CA.

For positive control of direct binding of ssDNA to the c-BN surface, a carboxyl terminated ssDNA-strand in combination with the EDC-protocol was used: COOH–C_6H_{12}–CCC CTG CA.

All DNA strands are labeled at the 5′ end with an ALEXA 488 fluorescent label to provide the option of confocal microscopy.

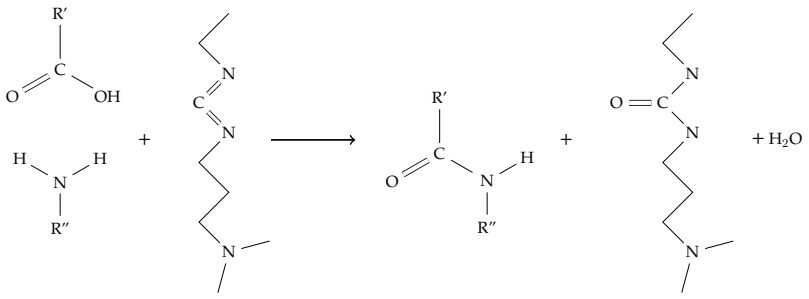

Figure 2.3: The EDC protocol: A carboxyl- and an amine-terminated molecule form a peptide bond through the mediation of EDC.

Fatty Acid

For Fatty Acid treatment, the hydrogenated c-BN thin films were covered with a droplet of 10-undecanoic acid and then illuminated by light with a wavelength of 254 nm for 20 h inside an EPROM eraser box from LAWTRONICS by a light from PHILIPS TUV G4T4 4 W lamp (2.5 mW/cm^2). This was done inside a nitrogen atmosphere in a glove box to avoid unwanted side reactions and oxidation of EDC.

The samples were then rinsed thoroughly with 10 % Sodium Dodecyl Sulfate (SDS), an anionic surfactant that disrupts non-covalent bonds and can be used for both cleaning of fatty surfaces and denaturation of proteins, forcing them to lose their conformation. This way, all remaining and unbound Fatty Acid molecules were washed off the surface.

In a next step, the samples were incubated with 50 µl of ALEXA 488-labeled ssDNA (1.2 µg) and 1 mg EDC in 25 mM 2-(N-morpholino)ethanesulfonic acid (MES)-buffer (pH 6) for 2 h at a temperature of 6 °C to let the EDC-protocol activate the coupling of the primary amine group from the ssDNA and the carboxyl group from the Fatty Acid (see Figure 2.4).

The functionalized samples were finally washed with SDS and Saline-sodium citrate (SSC) to remove physisorbed DNA and EDC by breaking non covalent bonds. They were then washed with deionized (DI)-water to remove the SDS and SSC.

Protocols for this type of linkage can be found in numerous publications[5,14,15].

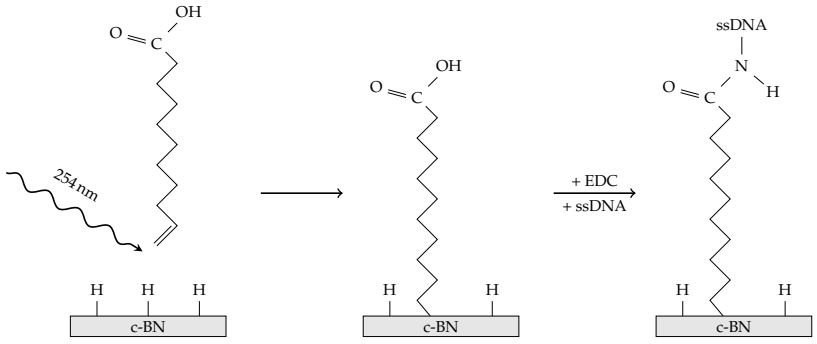

Figure 2.4: Fatty Acid reaction: UV-light breaks the double bond of 10-undecanoic acid which then forms a stable bond with the c-BN surface. DNA can then be bound to the carboxyl-group of the Fatty Acid by mediation of EDC.

Diazonium

The diazonium coupling was performed with freshly hydrogenated c-BN samples in 5 mM 4-carboxy-diazonium tetrafluoroborate in 100 ml HCl (0.1 M) in a three neck flask under nitrogen atmosphere. The temperature of this solution was 60 °C and coupling time 1 h, as described in literature[16–18].

Samples were rinsed with SDS and SSC, then with DI-water before the EDC-Protocol with 50 µl of ALEXA 488-labeled ssDNA (1.2 µg) and 1 mg EDC in 25 mM MES-buffer (pH 6) was performed for 2 h at a temperature of 6 °C to bind ssDNA to the linked Diazonium.

A schematic overview over the binding steps can be seen in Figure 2.5.

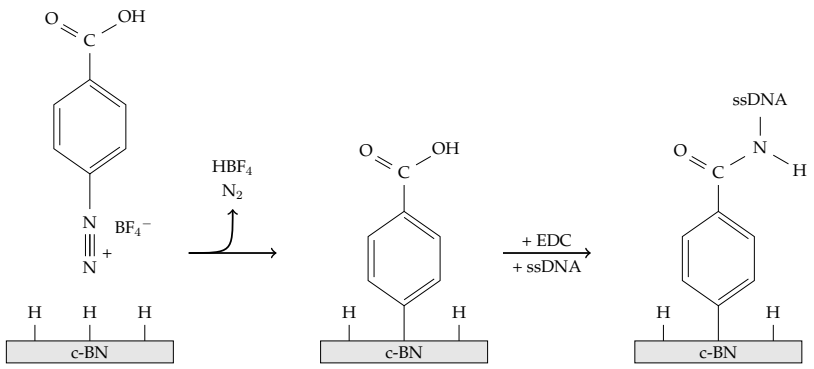

Figure 2.5: Diazonium reaction: 4-carboxy-diazonium tetrafluoroborate binds to the c-BN surface, thus setting hydroxyborate and nitrogen gas free. The carboxyl-group of Diazonium then serves as functional group for the EDC-mediated attachment of ssDNA.

Zero-length cross-linker

To investigate whether direct coupling of DNA to the surface of c-BN is possible, carboxyl terminated ssDNA was used as positive and NH_2 terminated ssDNA as negative control. A droplet containing 1 mg EDC in 25 mM MES-buffer (pH 6) and 50 µl of ALEXA 488-labeled COOH- and NH_2-ssDNA (1.2 µg), respectively, were placed on the hydrogenated c-BN samples and left to react at 6 °C for 2 h.

The samples were then washed at 60 °C in SDS for a total of 24 h with exchange of SDS after 1, 2, 4, and 12 h.

2.3 Sample analyzation

For this study, analyzation of the samples needed to be both surface sensitive to gain information on the functionalized surface and bulk sensitive to gain information on the quality of the c-BN thin film. Therefore a set of analyzation techniques was chosen which meet both requirements.

X-Ray Photoelectron Spectroscopy

X-ray Photoelectron Spectroscopy (XPS) is a surface sensitive method for chemical analysis. Its working principle is based on the Photoelectric Effect (see Figure 2.6) which was first described by Albert Einstein in 1905[19]. It describes the fact, that irradiating a sample with photons of energy E_{photon} will free electrons with a kinetic energy E_{kin}. Equation 2.1 links photon energy and kinetic energy in a way, that the binding energy E_{B} can be calculated if the photon energy $h\nu$ and the work function of the spectrometer Φ_{spekt} are known and E_{kin} is measured.

$$E_{\mathrm{kin}} = h\nu - E_{\mathrm{B}} - \Phi_{\mathrm{spekt}} \tag{2.1}$$

In order to induce the Photoelectric Effect in XPS, the sample is irradiated under Ultra High Vacuum (UHV) conditions with soft X-Rays and the emitted electrons are being analyzed with respect to their energy (see Figure 2.6). Since the penetration depth of soft X-Rays is limited to several µm, interaction with atoms is only possible in the surface region of the sample. The emitted electrons can only leave the sample without energy loss if they do not interact and/or collide with the atoms surrounding them. As a consequence, the analyzing depth for XPS is in the range of the inelastic mean free path length of the electrons in the sample.

Once the electrons emerging from within this inelastic mean free path length have left the bulk sample, they are being accelerated towards the electric lens system of the analyzer. This system acts as an energy "window" that only allows electrons within a range of energy, the pass energy E_{pass}, to pass. This pass energy can be varied from zero up to the photon energy. Only electrons with an energy higher or equal to E_{pass} can enter the analyzer and will be detected. Thus, by varying the pass energy, electrons with known kinetic energies can selectively be detected.

Analyzing these electrons, information about the binding energy can be gathered. Since theses energies are unique for every type of atom, the peaks in the energy spectrum can be assigned not only to the specific

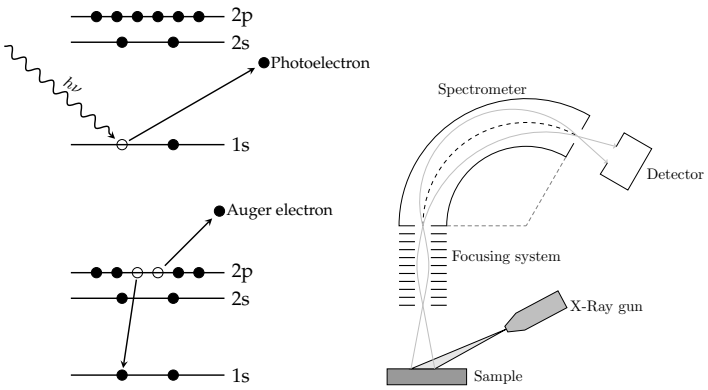

Figure 2.6: Left: Photoelectric Effect and Auger Effect. Right: Schematics of a general XPS system.

elements and their distinctive orbitals but also to the chemical state of the sample.

Analyzing the peak height, area, position and peak separation energies between distinct peaks allows semi-quantitative analysis of the samples.

In this work, XPS measurements were performed using PERKIN ELMER ESCA Spectrometer with monochromatic Al $K\alpha$ radiation of 1486.6 eV. Spectra were calibrated by setting the gold reference $\mathrm{Au}_{4\mathrm{f}_{7/2}}$ to 84.0 eV or, where gold references were not available, setting the $\mathrm{C}_{1\mathrm{s}}$ binding energy reference to 285.0 eV as described in literature[20]. The spectra calibrated in this way are marked in the text.

Peak intensities in XPS depend on many factors. The number of photoelectrons I per second that are emitted during XPS analysis is given by the equation:

$$I = nf\sigma\theta y\lambda AT \tag{2.2}$$

where n is the number of atoms per cm^3 in the sample, f the X-Ray flux in photons/cm^2, σ the photoelectric cross-section for the atomic orbital of interest in cm^2, θ is the emission angle, y is the efficiency in the photoelectric process for the formation of photoelectrons, λ is the inelastic mean free path length of electrons in the sample, A is the detection area of photoelectrons on the sample and T is the detection efficiency for electrons emitted from the sample[21].

This shows that the peak area for quantitative analysis is composed of different contributions. In this work all spectra were gained with the same analyzer setup to allow comparison and analysis of peak areas and intensities.

The relative concentrations of constituents in the XPS-spectra were calculated using peak area sensitivity factors as listed in[22] and Equation 2.3[21]. This states, that the atom fraction c_x depends on its XPS peak area I_x by the atomic sensitivity factor S_x in relation to the sum of all peak areas divided by their atomic sensitivity factors.

$$c_x = \frac{\frac{I_x}{S_x}}{\sum_i \frac{I_i}{S_i}} \tag{2.3}$$

This holds true for any XPS peak that results from homogenous distributed atoms within the analyzation depth of XPS. For surface treated samples and for contaminations that are not within the film but only at the surface of the sample, the calculation of the atomic fraction c_x needs to be adopted. The model explained in the following emanates from the assumption that in the thin film, boron and nitrogen are present at a ratio of 1:1.

Measuring depth d of XPS is the sum of $\cos\theta$, where θ is the emission angle, and λ, the inelastic mean free path length of the bulk substrate[23].

$$d = \lambda \cos\theta \tag{2.4}$$

For inorganic compounds, the inelastic mean free path length is given by the formula of Tanuma, Powell and Penn[24]:

$$\lambda = \frac{E}{{E_p}^2 \left[\beta \ln(\gamma E) - \frac{C}{E} + \frac{D}{E^2}\right]} \tag{2.5}$$

where E is the electron energy, $E_p = 28.8\sqrt{N_\nu \rho / M}$ with N_ν as the number of valence electrons per atom (3 for boron and 5 for nitrogen), the density ρ and the atomic weight M. β is given by

$$\beta = 0.0216 + \frac{0.944}{\sqrt{{E_p}^2 + {E_g}^2}} + 0.000739\rho \tag{2.6}$$

with the band gap E_g. The parameters C and D for inorganic materials are defined as

$$C = \frac{0.065}{U^2} - \frac{0.130}{U} + 1.11 \tag{2.7}$$

$$D = \frac{1.91}{U^2} - \frac{5.12}{U} + 35.3 \tag{2.8}$$

and $U = \rho N_\nu / M$. Taking these formulas into account, the inelastic mean free path length can be calculated and results for c-BN in a value of approximately 2.64 nm. With an emission angle of 30° this leads to an effective measuring depth of 2.19 nm. Incorporating the interatomic distance of c-BN as 1.57 Å [25,26], the measuring depth allows to analyze a total of almost 14 monolayers of c-BN.

Signals arising from the sample surface thus need to be seen as if they possessed almost 14 times the intensity of the bulk signals if assumed that they arise from the topmost monolayer only.

Core level spectra have been investigated with the help of non-linear least squares curve fitting with Gaussian types of function as described in literature [20]. The baseline correction was performed using a simple spline baseline subtraction.

The surface coverage of linker molecule was calculated from the carboxyl peak contribution in the C_{1s} core level spectrum in XPS in relation to the corrected B_{1s} and N_{1s} peak areas, thus determining the carboxyl surface concentration. With the given atomic density of 1.68×10^{23} cm^{-3} [27] for c-BN, the surface density can be determined with the help of (atomic density)$^{2/3}$ as described in literature [28] to be 3.04×10^{15} cm^{-2}. Since every linker molecule contains only one carboxyl group, the surface coverage can be determined by multiplying the carboxyl surface concentration with the surface density.

For the calculation of DNA surface coverage, the sulfur peak is taken as reference. Every ALEXA 488 label contains two sulfate groups, thus the sulfur surface concentration needs to be multiplied with the surface density of c-BN and the result is divided by two to yield the DNA surface coverage.

Confocal imaging

The principle behind fluorescence microscopy is that the sample containing fluorophores is illuminated with light of a distinct wavelength. The fluorophores absorb this light and emit light of lower wavelengths. By separation of the illumination and the weaker emission light with special filters, pure fluorescence light can be detected without interference from illuminating light.

Confocal Fluorescence Microscopy uses point illumination of a certain spot only and makes use of a pinhole to filter out light that comes from

an out-of-focus region. Subsequently the surface of the sample is scanned rather than illuminating the whole sample with light. This way, only fluorescence close to the focal plane is detected which increases the resolution and allows 2D and 3D images but at the same time decreases the signal intensity.

To assure that the measured light intensity comes from the fluorophores and is not an artifact of the measurement, a region on the sample can be photo-bleached. This region is illuminated with high intensity light for several times, so that photochemical destruction of the fluorophores takes place. The degradation of fluorophores is indicated by a darkened region and proves that fluorophores are present and can be destroyed by high intensity light.

For this work, a ZEISS LSM 510 META one-photon CLSM device with a 30 mW air cooled argon laser (set to 45 % max. power, 5.7 A) was used. To excite the ALEXA 488 labels in the samples, the 488 nm line of the laser was used. The collected fluorescence from the sample then passed a 505 nm lowpass emission filter to the photomultiplier tube.

Images were recorded at 10 % transmission to avoid photobleaching during acquisition. For the bleaching process, the region of interest was exposed to 100 % transmission for 10 scans.

Contact Angle and Surface Free Energy

Contact angles of c-BN, h-BN and NCD were measured using DATAPHYSICS OCA 15plus optical contact angle measurement device. The average of three measurements was used to calculate the mean value for the contact angle.

Contact angles were measured after 5, 10, 20 min, 1, 12, 24, 36 and 48 h after hydrogenation to gain information on the stability of the hydrogenated surface. The samples were stored at room temperature in MES-buffer in the interim time.

For the calculation of Surface Free Energy (SFE), several considerations were taken into account. The SFE of any solid is described by Young's equation[29]

$$\sigma_s = \sigma_{sl} + \sigma_l \cdot \cos\theta \tag{2.9}$$

where σ_s is the Surface Free Energy of the solid, σ_{sl} the SFE of the solid–liquid interface, σ_l the SFE of the liquid and θ the contact angle between sold and liquid.

Following Ownen's and Wendt's theory[30], the surface energy of any solid or liquid phase can be split up into two components: A dispersive (σ^D) and a polar (σ^P) part:

$$\sigma_s = \sigma_s^D + \sigma_s^P \tag{2.10}$$

$$\sigma_l = \sigma_l^D + \sigma_l^P \tag{2.11}$$

Taking into account the polar and dispersive forces for surface energy calculations, the following formula was proposed:

$$\sigma_{sl} = \sigma_s + \sigma_l - 2\left(\sqrt{\sigma_s^D \cdot \sigma_l^D} + \sqrt{\sigma_l^D \cdot \sigma_l^P}\right) \tag{2.12}$$

Combining Equation 2.9, 2.10, 2.11 and 2.12, the theory of Owen, Wendt, Rabel and Kabele[31] provides an equation in the form of a linear equation:

$$\frac{(1+\cos\theta)\cdot\sigma_l}{2\sqrt{\sigma_l^D}} = \sqrt{\sigma_s^P}\cdot\sqrt{\frac{\sigma_l^P}{\sigma_l^D}} + \sqrt{\sigma_s^D} \tag{2.13}$$

For liquids with known dispersive and polar components, the contact angle can be measured and the SFE can be interpolated by plotting $\frac{(1+\cos\theta)\cdot\sigma_l}{2\sqrt{\sigma_l^D}}$ versus $\sqrt{\frac{\sigma_l^P}{\sigma_l^D}}$. The slope $\sqrt{\sigma_s^P}$ and intercept $\sqrt{\sigma_s^D}$ of the regression line can be found from the linear equation of the regression line. The sum of their square represents the SFE of the system.

For the calculation of the SFE of c-BN, 4 liquids were used: DI-Water, Ethylene Glycole, Dimethoxy Silane and Diiodomethane. For these liquids, polar and dispersive components are known[32] and they differ in these components. Absolute values are listed in Table 2.1. For each liquid, a new hydrogenated sample was used and three measurements were taken to average the contact angle.

Table 2.1: Surface Free Energy, polar and dispersive components of the liquids used for SFE-calculations of cBN

	σ_l	σ_l^P	σ_l^D
Water	72.8	51.0	21.8
Ethylene Glycole	48.0	19.0	29.0
Dimethoxy silane	44.0	8.0	36.0
Diiodomethane	50.8	0	50.8

Atomic Force Microscopy

Atomic Force Microscopy (AFM) was used to determine the surface roughness of the thin films and their morphology. The determination of a surface's roughness plays an important role for surface functionalization since high roughness values favor physisorption and allow trapping of molecules easily. This hinders the analyzation of binding, since it cannot be distinguished between covalently bond and physisorbed or trapped molecules.

The Atomic Force Microscope (AFM) used for this work was driven in tapping mode. For this mode, a cantilever oscillates near its resonance frequency, though not coming into contact with the sample surface itself. In close distance to the surface, interactions between the cantilever and the surface force the amplitude of oscillations to decrease. To maintain the oscillation frequency, the height of the cantilever tip is adjusted. The cantilever then scans the surface and a morphology image can be assembled by the individual height adjustments necessary for the compensation of changes in oscillation.

The advantage of the tapping mode is its high lateral resolution and the reduction of damage to the sample. The absence of contact between cantilever tip and sample also reduces the amount of contamination.

Fourier Transformed Infrared Spectroscopy

Fourier Transformed Infrared Spectroscopy (FTIR) is a widely used technique for the characterization of Boron Nitride samples. Due to the characteristic vibration modes of both c-BN and h-BN, FTIR can be used to gain information about the volume fraction of cubic phase BN in the thin film. For this work, ex situ transmission spectra were performed using a NICOLET 8700 FT-IR device with a scan range from 400 to 4000 cm^{-1}, a resolution of 2 cm^{-1} and a KBr beam splitter. Before every scan, an NCD background scan was performed and then subtracted from the actual c-BN scan since the c-BN thin films were grown on NCD. Peak resolve was performed using OMNIC Software and Lorentzian fitting to find the peak positions, Full Width at Half Maximum (FWHM) and intensities of the peak contributions.

For the calculation of the cubic phase volume fraction c_{cBN}, the following formula was used[9]:

$$c_{\mathrm{cBN}}\% = \frac{I_{\mathrm{cBN}}}{I_{\mathrm{cBN}} + I_{\mathrm{hBN}}} \tag{2.14}$$

with the intensity I_{cBN} of the c-BN transversal optical (TO) phonon and the intensity I_{hBN} of the h-BN contribution.

Since transmission mode FTIR mainly reveals information on the bulk sample, investigating the surface functionalization with transmission mode is difficult. The thin functionalization layer of several nanometers gives rise to only small peaks in the transmission spectrum. It is also not possible to distinguish between signals arising from the functionalized c-BN surface and those arising from the (possibly) functionalized back-side of the sample, the untreated silicon substrate. For this case, Grazing Angle Attenuated Total Reflection (GATR) would be useful, since it gives information on the surface af a sample only. Unfortunately the GATR device was out of order in the time of this work and could not be repaired in time to make extensive use of this powerful technique.

For this work, information on the functionalized surfaces therefore was gained using XPS and fluorescence microscopy. FTIR was used for the determination of the cubic phase volume content of samples deposited in double sided polished substrates. However, as GATR was available again towards the end of this study, it was used to determine the cubic phase content of samples deposited on single sided polished substrates.

3 Results & Discussion

The obtained NCD thin films showed surfaces without major contaminations. As can be seen from Figure 3.1, except for oxygen contamination the XPS scan shows no impurities. The O_{1s} peak contribution has, if assumed that the oxidation comes from the surface alone and is not present in the bulk, a relative content of 4.8 at.%. This implies, that oxygen comes not from thin film deposition but is an ex situ contamination. This oxygen contamination may either stem from oxidized diamond at the surface or arise from dust particles and oxygen containing hydrocarbons which gravitated on the surface since handling of the samples did not take place in a cleanroom.

The XPS scan of the thin film shows no signals from the silicon substrate which proves that the film covers the substrate thoroughly.

XPS of c-BN thin films as seen in Figure 3.2 a) show the two distinct peaks for N_{1s} and B_{1s} at 398.4 eV and 190.8 eV respectively. The boron to nitrogen ratio B/N of 1.04 indicates a slight surplus of boron, possibly due to the formation of nitrogen vacancies[27].

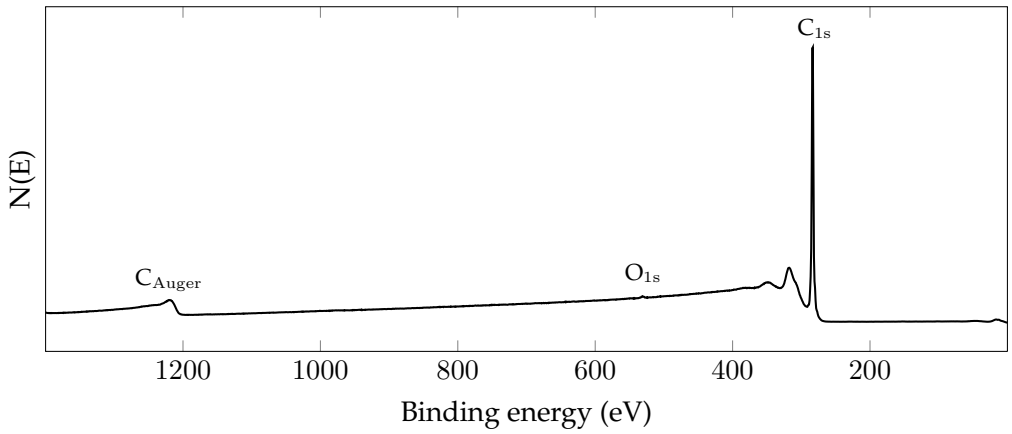

Figure 3.1: XPS spectrum of the ex situ as-prepared NCD thin film prior to c-BN deposition. C_{1s} and C_{Auger} peaks are the most prominent.

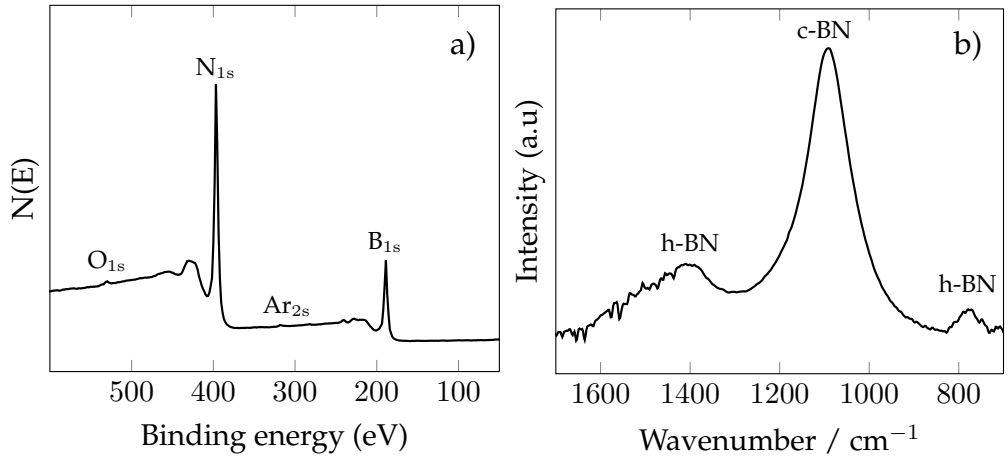

Figure 3.2: a) XPS spectrum of an as-prepared c-BN thin film. N_{1s} and B_{1s} are the most prominent peaks, accompanied by minor contributions from O_{1s} , $Ar_{2p_{3/2}}$ (at 241.8 eV) and Ar_{2s} b) FTIR scan of c-BN in transmission mode. FWHM of c-BN-TO is 122.8 $cm^{-1}$and the cubic phase content is 78 %

Besides the two most prominent peaks, the spectrum comprises of an O_{1s} contribution at 531.8 eV with a relative content of 0.46 at.% in the bulk or 6.4 at.% at the surface. This may be due to residual oxygen in the deposition chamber during thin film growth (base pressure before growth was 1×10^{-8} mbar at 800°C) or due to oxygen present in the transfer between deposition chamber and analyzation chamber (pressure 2×10^{-7} mbar at room temperature).

Both $Ar_{2p_{3/2}}$ at 241.8 eV and Ar_{2p} at 319.5 eV prove that ion implantation occurred while film growth took place. This argon is removed during hydrogen plasma treatment as discussed later.

The FTIR scan (see Figure 3.2 b) indicates a high cubic phase volume fraction of 78 % in the thin film. Since the FTIR scan is taken in transmission mode, this gives general information about the film itself but only few information about the surface.

AFM scans of the NCD surface (Figure 3.3 a) showed the typical pattern of nanocrystalline diamond [33]. The root mean square roughness of this thin film is in the range of 13 nm at a total thin film thickness of approximately 100 nm.

The AFM scan after c-BN deposition (Figure 3.3 b) shows a root mean square roughness in the range of 10 nm. This indicates that the deposition proceeds almost uniformly. No major changes in surface roughness or morphology could be detected.

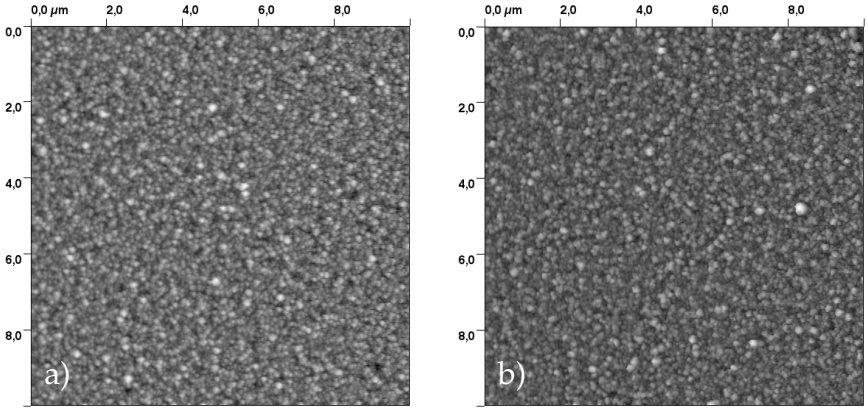

Figure 3.3: 1 x 1 µm AFM scans of a) NCD and b) c-BN. The root mean square roughness is 12.6 nm for NCD and 10.2 nm for c-BN respectively

During hydrogen plasma, silicon was deposited on the c-BN thin film. This can be seen from the XPS spectrum in Figure 3.4 a). Both Si_{2s} at 150.5 eV and Si_{2p} at 102.5 eV reveal, that 3.2 at% of the Boron Nitride surface is covered with silicon. This silicon may have its origin in the window of the hydrogenation chamber or in the silicon substrate which is sputtered during hydrogenation thus creating 1/30 monolayer of silicon on the substrate.

The carbon peak that occurs in the spectrum is due to the ex situ hydrogenation including the transport of the sample in ambient air and physisorbed particles at the sample surface. The oxygen peak at 532.0 eV presumably arises from these particles containing oxygen at the surface, but also is partly originating from the silicon which is present in its oxidized form, as the peak position at 102.5 eV shows[21]. In addition it arises from the slightly oxidized boron, as will be discussed later.

The XPS spectrum in Figure 3.4 (b) shows the plasmon region of the B_{1s} peak of the as-prepared c-BN sample and the hydrogenated sample. Four major peaks can be detected in this range: The B_{1s} peak at 190.8 eV, the $\pi \rightarrow \pi^*$ shake-up line at 199.0 eV, the Mo_{3d} peak at 230.2 eV and the $Ar_{2p_{3/2}}$ peak at 241.5 eV.

A decrease in the $\pi \rightarrow \pi^*$ shake-up line is caused by the etching of the topmost layers of the sample in the hydrogenation process. The h-BN layer that has been reported to be at the surface[11] is diminished by hydrogenation. This was also detected with FTIR, since the bulk content of the cubic phase increases for around 1.47 $\pm$0.4 % after hydrogenation.

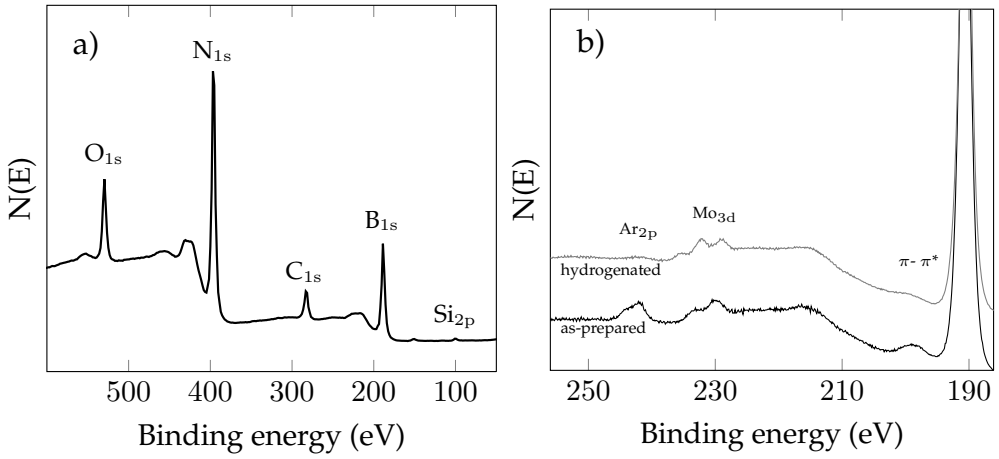

Figure 3.4: a) XPS spectrum of hydrogenated c-BN. Both oxygen and carbon contributions increase due to ex situ hydrogenation, as well as silicon deposition. b) B_{1s} plasmon region of as-prepared and hydrogenated c-BN. Argon is sputtered and the decrease in π-π* indicates etching of the topmost h-BN layer.

Argon is implanted in the c-BN film during deposition due to the N_2/Ar plasma. Argon ions are accelerated to the target and the sample because of the applied bias voltage during deposition. The argon present in the c-BN thin films investigated is located in the topmost layers, because it is removed while undergoing hydrogenation as can be seen in Figure 3.4 (b). The decrease of molybdenum in contrast to the argon decrease is very low, leading to the conclusion that molybdenum is present not only at the sample surface but within the film. The molybdenum arises from sputtering the sample holder and screws holding the substrates during deposition.

The valence band spectrum in Figure 3.5 supports the observation of a decrease in argon by hydrogenation since the Ar_{3p} contribution decreases in the valence band spectrum as well. In addition to this, an O_{2s} shoulder, positioned at 26 eV, and an O_{2p} shoulder, positioned at 7.0 eV, rise after hydrogenation indicating the oxidation of the surface. This oxygen derives from contaminations in the hydrogenation process, since c-BN possesses a high resistance to oxidation under ambient conditions[34] and therefore is unlikely to oxidize to this amount at room temperature. Residual gas in the hydrogenation chamber, which had a base pressure of 3×10^{-6} mbar before hydrogenation, may have lead to a mixture of hydrogen and oxygen plasma and thus to the oxidation of c-BN[35].

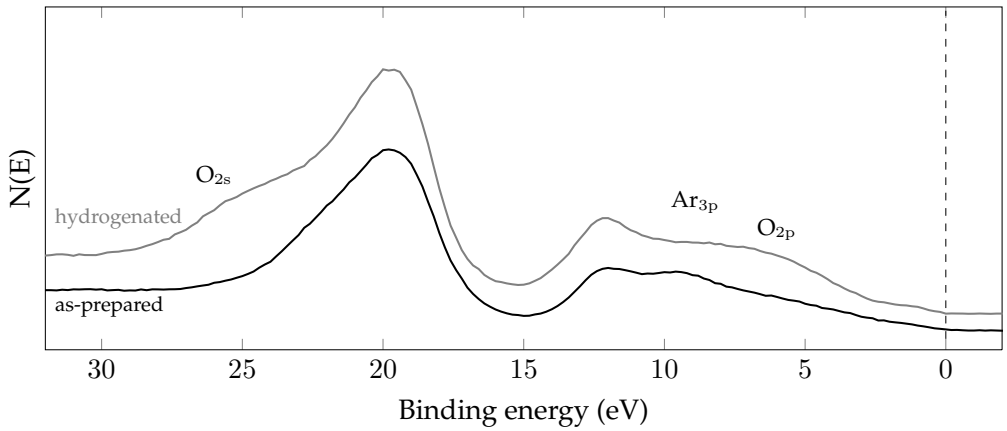

Figure 3.5: Valence band spectrum of as-prepared c-BN and hydrogenated c-BN. The hydrogenated spectrum shows O_{2s} and O_{2p} induced shoulders and a decreased contribution of Ar_{3p} .

Figure 3.6 depicts the core level spectra of B_{1s} and N_{1s} . The different stages of sample treatment before binding of linker molecule are shown. Open circles represent the acquired data, full lines the least square curve fitting results.

Both B_{1s} and N_{1s} peaks are composed of contributions from the sp^2 bonded h-BN and the sp^3 bonded c-BN. In addition to these two contributions, the B_{1s} core level scan of the hydrogenated sample contains a third contribution with its center at 192.3 eV which can be assigned to oxidized boron[35–37]. This is in agreement with the observations of the survey scan and the valence band spectrum. It is striking, that the N_{1s} core level scan does not show any oxidized contribution.

The ratio of B–O/B is 0.312 (assuming that the oxygen is at the surface only) which means that 31.2 % of boron at the surface of the sample contains B–O bonds after hydrogenation. Therefore, 15.6 % of the entire c-BN film surface is covered with oxygen.

The ratio of h-BN/c-BN for N_{1s} decreases from 0.396 in the as-prepared sample to 0.352 in the hydrogenated sample (Δ=0.044) and for B_{1s} it decreases from 0.351 to 0.298 (Δ=0.053), indicating that the top h-BN layers were only partially etched by the hydrogenation. This removal of hexagonal phase at the top layer surface can be confirmed with the relative increase in cubic phase content detected by transmission FTIR. The evaluated relative increase in cubic phase volume content for the hydrogenated sample is 0.8 % (from 71.62 % cubic phase in the bare c-BN film to 72.38 % in the hydrogenated film).

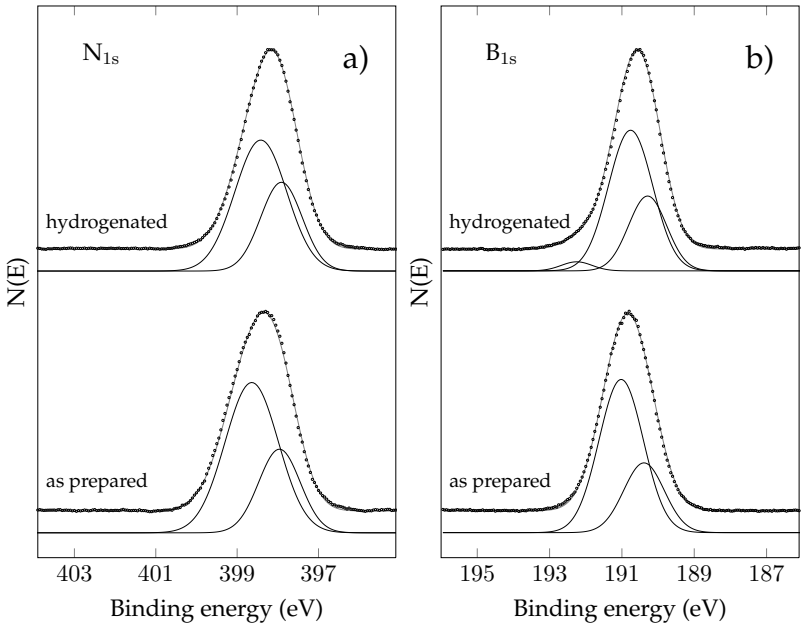

Figure 3.6: XPS spectra of N_{1s} (a) and B_{1s} (b) core level in c-BN thin films. Full lines show the contributions of a gaussian fitting procedure. For N_{1s} and B_{1s} , both cubic and hexagonal contributions are present. B_{1s} shows an oxidized boron contribution after hydrogenation.

The comparably small decrease of hexagonal phase and the deconvolution of both the as-prepared and hydrogenated B_{1s} and N_{1s} core level spectra reveal, that the sample contains hexagonal phase in the thin film itself and not mainly at the sample surface, since the topmost layers are etched by the hydrogen plasma. The core level spectra show, that the surface still contains a significant amount of around 30 % hexagonal phase Boron Nitride. It might as well be the case, that the hydrogenation with 3000 W microwave H-plasma is not powerful enough to remove this top layers.

3.1 Contact Angle and Surface Free Energy

The contact angle of c-BN, h-BN and NCD versus time was measured with a droplet of 1 µl DI-water after fresh hydrogenation of the samples. The resulting contact angles are shown in Figure 3.7. It can be seen, that the surface hydrogenation of NCD stays at a stable value of approximately 87° for the first 60 minutes in MES buffer and decreases gradually only after this time. This indicates that there are no major changes in the hydrogenation termination of the diamond surface.

Both c-BN and h-BN start at an initial contact angle of approximately 36° but show a rapid decrease within the first 20 min. The contact angle then stabilizes around 27° for c-BN and around 18° for h-BN. This indicates, that the hydrogenation of c-BN and h-BN is not as stable in MES buffer as the hydrogenation of NCD films. Processes at the Boron Nitride surface change the properties of the termination layer in a way, that the contact angle decreases and the surface becomes more hydrophilic.

Since the surface properties for c-BN and h-BN change rapidly, the timescale for functionalization of the hydrogenated surfaces lies in the range of several minutes after hydrogenation. Keeping this in mind, for this work all functionalizations were performed immediately after hydrogenation thus keeping the time interval between hydrogenation and functionalization as short as possible (between 4 and 7 min) and reducing the effect of degradation of the hydrogen surface termination.

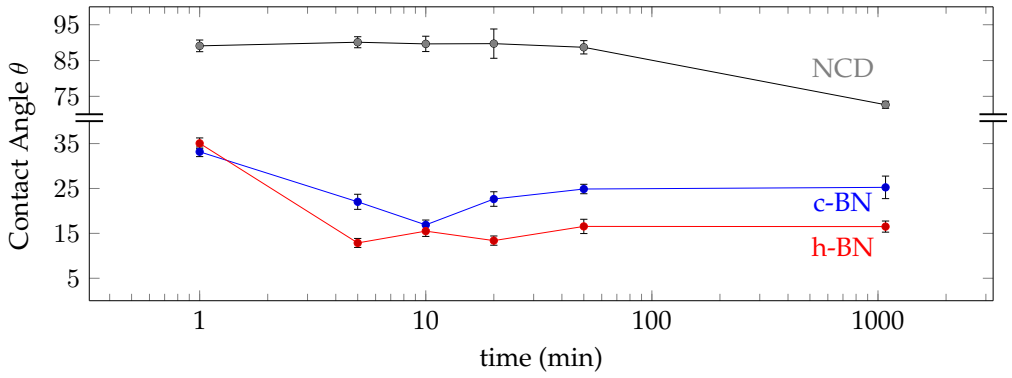

Figure 3.7: Contact Angle of NCD, c-BN and h-BN over time. Three measurements were taken for every data point. The zero point of the time scale marks the removal of samples from the hydrogenation chamber.

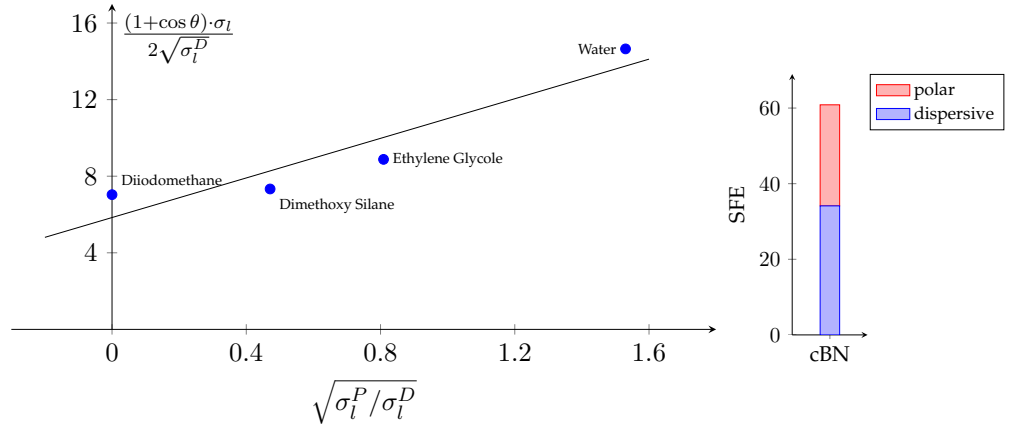

Figure 3.8: Left graph: Determination of Surface Free Energy and polar and dispersive components with the help of contact angle θ and the polar (σ_l^P) and dispersive (σ_l^D) components of four liquids: Diiodomethane, Diethoxy Silane, Ethylene Glycole and Water. Right graph: The bar graph shows polar and dispersive contributions to the Surface Free Energy.

The Surface Free Energy was determined with the help of the square intercept and the square slope of the regression line from Figure 3.8 as explained in the Materials & Methods chapter of this work. The calculated Surface Free Energy of c-BN is 60.86 mJ/m^2 with a polar contribution σ_l^P of 26.73 mJ/m^2 and a dispersive contribution σ_l^D of 34.13 mJ/m^2. This result is consistent with SFE for Boron Nitride from literature[38]. In respect to diamond, c-BN exhibits a very high polar contribution which can easily be seen from the lower contact angle of water, indicating that c-BN is hydrophilic whereas diamond is hydrophobic. This corresponds with the ionic character of c-BN due to the differences in electronegativity of both elements and favors the attachment of different linker molecules which are soluble in aqueous solutions such as diazonium salts.

3.2 Fatty Acid linker

Fatty Acid linking resulted in evaluable fluorescence under the confocal microscope as can be seen from Figure 3.9. Image (a) shows Fatty Acid linked DNA on c-BN before photo-bleach, (b) shows the same area after photo-bleach. The photo-beached rectangular region of interest in (b) is perceivable clearly. This indicates, that fluorophores could be bleached thus the presence of fluorophores at the surface is given. The EDC protocol therefore was able to establish a peptide bond between carboxyl groups of the Fatty Acid and the amine group at the 5' end of DNA. To quantify this, XPS analysis was performed.

The intensity of the C_{1s} peak in the survey spectrum of c-BN with Fatty acid significantly increased, indicating the presence of Fatty Acid at the sample surface. The C/c-BN ratio increases by a factor of 4.2 after Fatty Acid linking. This increase in C_{1s} and the corresponding decrease in B_{1s} and N_{1s} by Fatty Acid coupling indicates that a dense layer of linker molecules formed on top of the c-BN.

After coupling of DNA to the Fatty acid, the increase of C/c-BN has a factor of 1.7 in respect to the Fatty Acid and only a small corresponding decrease in B_{1s} and N_{1s} peak intensities indicating that binding DNA to Fatty Acid creates a loose layer of DNA. On the one hand, this can be an indicator for a small surface coverage. On the other hand, it can indicate that DNA strands do not form a densely layered structure but due to the sustained shape of DNA rather form a mesh of DNA than a highly oriented layer.

Core level spectra of N_{1s} and B_{1s} (see Figure 3.10) give valuable information on the binding nature of Fatty Acid to c-BN. Open circles in the plots represent the acquired data, solid lines the result of a least square

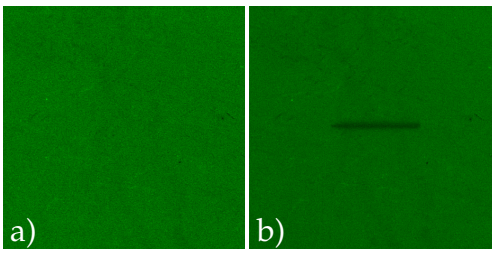

Figure 3.9: a) Fatty Acid linker and DNA before photo-bleach b) Fatty Acid linker and DNA after photo-bleach. The dark region in b) shows the photo-bleached fluorophores from ALEXA 488 label.

curve fitting procedure. The ratio of h-BN/c-BN contributions changes in the spectra due to the fact, that for every scan different samples with different cubic phase contents were used.

Deconvolution of the N_{1s} core level spectrum of hydrogenated c-BN (i) shows the split up of the peak into two components: c-BN and h-BN, as described before. The ratio of h-BN/c-BN is 0.31 which corresponds to the cubic phase content of 72.1 % as obtained from FTIR results. B_{1s} core level spectrum shows a similar ratio and exhibits a B–O contribution as described previously.

On binding Fatty Acid (ii), a third component adds to the N_{1s} peak: The N–C contribution at 399.3 eV[5,36,39]. Since there is no amine bond present in Fatty Acid, this N–C contribution shows that the Fatty Acid linker bound to the nitrogen from the c-BN surface. This can also be seen from a C–N contribution in the C_{1s} spectrum, which is located at 286.4 eV[35,40]. A corresponding B–C contribution from B_{1s} peak, which is to be located around 189.6 eV[36,40,41], is not present in the core level spectrum indicating that, other than described in literature[5,27], the linker in this work does only bind to nitrogen.

The C_{1s} core level spectrum shows a COOH contribution at 288.9 eV[42] and a C–N contribution at 286.4 eV[35,40] but no C–B contribution around 283.6 eV[35,41]. This confirms the theory that Fatty Acid in this work did only bind to nitrogen from the c-BN surface and not to boron.

In the B_{1s} core level spectrum, an oxidized component at 192.3 eV for the hydrogenated c-BN (see (i) in Figure 3.10) is present as described previously. This oxidized component increases on binding Fatty Acid to the c-BN surface from a B–O/B ratio of 0.312 to a B–O/B ratio of 0.952 if B–O is assumed to be present at the surface only and not within the film. Other than described in literature, the boron from the c-BN top layer seems to establish an oxygen bond and creates a B–O terminated surface.

The h-BN/c-BN ratio slightly shifts to 0.44 because the cubic phase content for this sample is 58.4 % only. Knowing that ever Fatty Acid linker on c-BN holds one single carboxyl group (see Figure 2.4), the COOH contribution from C_{1s} at 288.9 eV[42] allows to calculate the surface coverage of Fatty Acid on c-BN. Correlating the C–N contribution from N_{1s} to the c-BN surface as crosscheck, since one amine bond can be established per Fatty Acid molecule at the surface, a Fatty Acid surface coverage of 1.8×10^{14} Fatty Acid molecules per cm^2 is given.

The coupling of DNA to Fatty Acid linker showed a generally small decrease in the intensities of N_{1s} and B_{1s} spectra. In comparison to the

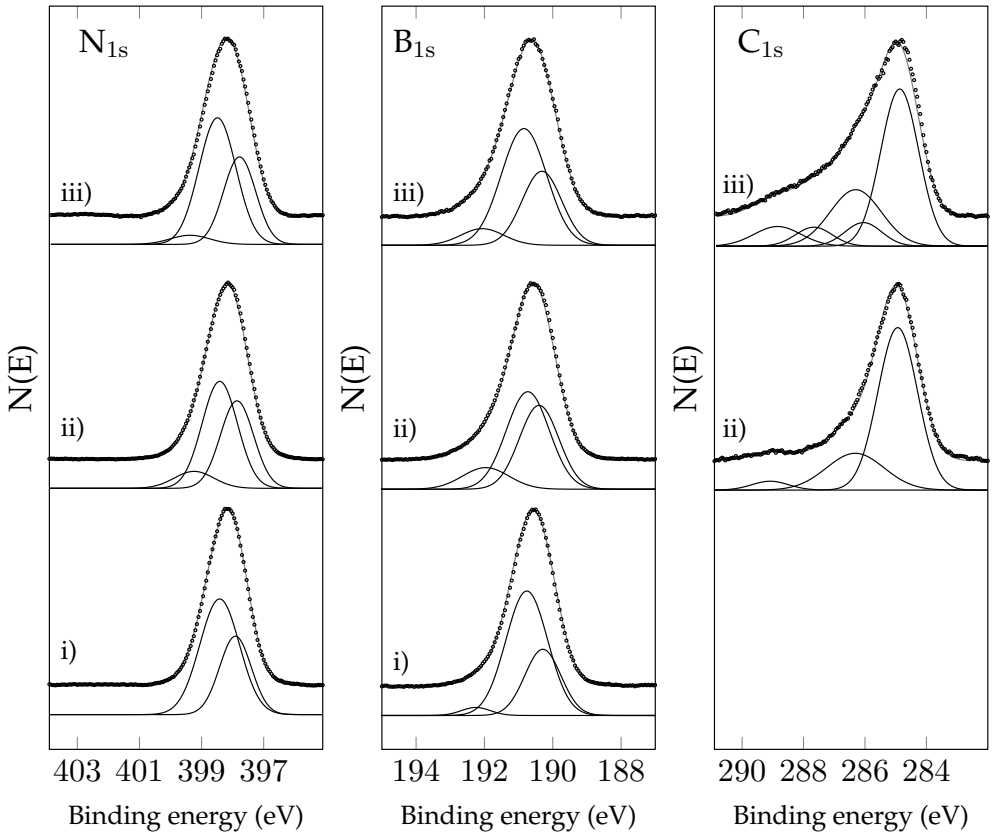

Figure 3.10: XPS core level spectra of Fatty Acid on cBN. i) hydrogenated c-BN, ii) Fatty Acid bound to c-BN, iii) DNA linked to Fatty Acid on c-BN.
For both N_{1s} and B_{1s} , sp^2 and sp^3 contributions are present. N_{1s} i) and ii) show an N–C contribution. B_{1s} exhibits a B–O contribution. C_{1s} ii) includes COOH and C–N contributions and C_{1s} iii) gives possible peak contributions for C–C, C–N, C=N, C–O and C=O. All spectra are normalized to 100 % intensity.

decrease after Fatty Acid linkage, this decrease was minor. This may be due to the relatively compact Fatty Acid layer on top of c-BN and a loose layer of DNA. The DNA surface coverage described later will support this claim.

The N_{1s} core level spectrum (iii) in Figure 3.10 showed a decrease in the N–C/N ratio. This relative decrease corresponds to the decrease in number of amine-groups present in the DNA and the label in relation to the alkene-bonds in DNA and label. The B_{1s} core level spectrum shows no significant change except its overall decrease in intensity. The oxidized form of boron does not change in relation to the hexagonal and cubic phase. The ratio of h-BN/c-BN in this sample is 0.37 corresponding to a

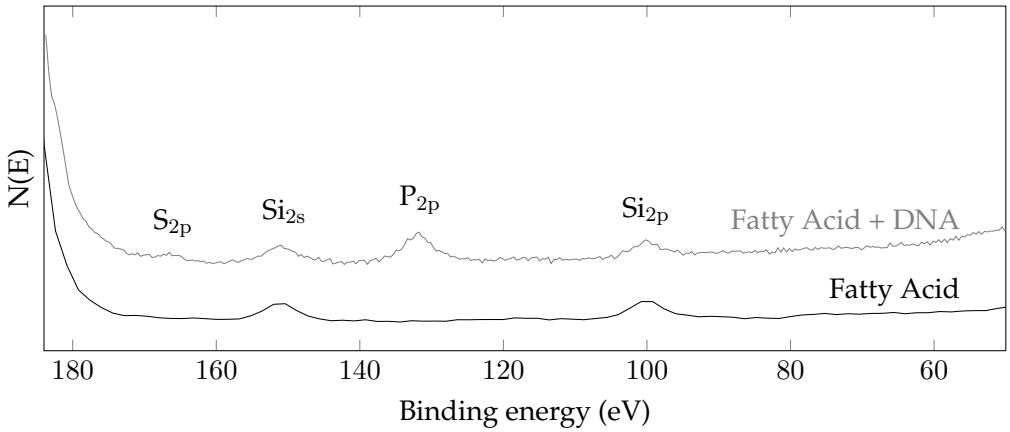

Figure 3.11: XPS spectra of Fatty Acid linker on c-BN and Fatty Acid bound to DNA on c-BN. The silicon contamination originates from hydrogenation and contaminated DNA, sulfur from the ALEXA 488 label and phosphor from phosphate groups within the DNA itself.

cubic phase content of 64.8 % as detected by FTIR.

C_{1s} core level spectrum and its fitting result as given in Figure 3.10 (iii) shows the Gaussian peaks of possible contributions to the C_{1s} spectrum. The amount of different binding types of the carbon atom in linker, DNA and label such as C–C, C=C, C–O, C=O, C-N, C=N, COOH and further more makes a distinct splitting of the peak into its components difficult. The fitting results showed in the spectrum therefore only give a set of the most prominent contributions: C–C at 285.0 eV, C–N at 286.4 eV, C–O at 286.7 eV and C=O at 287.8 eV. Since these peak contributions give a lot of margin for interpretation, the focus on evaluation lies upon the remaining core level spectra.

Figure 3.11 shows the enlarged region between 180 eV and 60 eV for Fatty Acid and a fine scan of DNA bound to Fatty Acid on c-BN. Silicon contaminations due to hydrogenation and contaminated DNA, as described earlier in this work, can clearly be seen from Si_{2s} at 150.5 eV and Si_{2p} at 100.1 eV. The sulfur S_{2p} peak originates from the fluorescent ALEXA 488 label attached to the 3' end of the DNA which contains two SO_3^- groups. The P_{2p} peak arises from the phosphate groups in the DNA. For the base sequence used in this work (CCC-CTG-CA), 8 phosphate groups are present. The ratio of P/S hence should be 4/1. Evaluation of the peak areas showed, that the experimental ratio is 5.3/1 which is consistent with the theory if the error and noise of such small peaks is taken into consideration.

The calculation of surface coverage for DNA on Fatty Acid linker can be investigated, since each ALEXA 488 label contains 2 sulfate groups and each label is bound to one single strand of DNA. The S_{2p} peak shown in Figure 3.11 offers the possibility to relate the S_{2p} peak to the c-BN surface and thus to calculate the DNA surface coverage. This gives a surface coverage of 7.55×10^{12} DNA molecules per cm^2.

3.3 Diazonium linker

The linkage of DNA to Diazonium showed fluorescence under the confocal microscope as can be seen from Figure 3.12. Image (a) and (b) show the negative control of Diazonium and DNA on the c-BN surface, but without the EDC linker, so that no nucleophilic substitution between linker and DNA took place and no peptide bond was formed. Images (c) and (d) represent Diazonium and DNA linked with the help of the EDC-protocol. The difference in fluorescence intensity is easily visible due to the bright color for the positive control, indicating a lot more fluorophores present in this sample and thus showing that more DNA is present.

Photo-bleaching for the negative control (b) showed that at the surface still DNA and fluorophores are present, since the rectangular region of interest that was bleached at 100 % illuminating light intensity shows a decrease in emission light intensity. This indicates that washing after DNA exposure was not effective enough and physisorbed DNA is still present at the sample surface. For washing, the well established protocol from diamond functionalization was adapted. Since c-BN exhibits a high polar contribution in Surface Free Energy, as shown in section 3.1, and NCD only possesses a small polar contribution[42], the effect of physisorption of charged molecules is much higher for c-BN than for NCD. Hence washing time of c-BN should be prolonged for further experiments.

For the positive control, photo-bleaching showed a bleached region of interest as well as can be seen from image (d). The bleached region is not entirely black, indicating that exposing this region to 100 % illuminating light intensity was not sufficient to destroy all fluorophores. Increasing

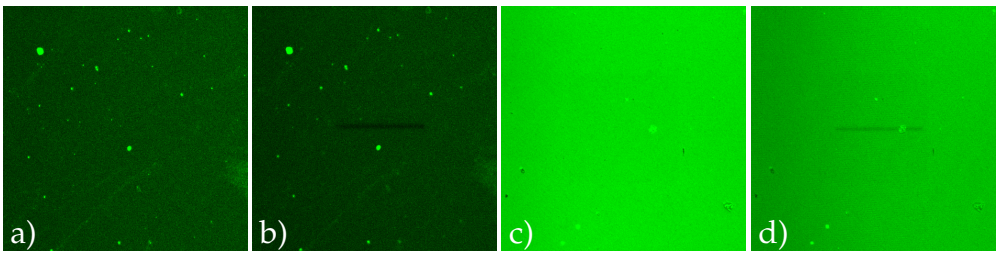

Figure 3.12: a) Negative control: Diazonium and DNA on c-BN before photo-bleach b) Negative control: Diazonium and DNA on c-BN after photo-bleach, c) Positive control: Diazonium and DNA before photo-bleach, d) Positive control: Diazonium and DNA after photo-bleach

the number of bleaching scans would resolve this problem but would make a comparison between different bleaching results of the same batch difficult.

The XPS core level spectra of Diazonium linked DNA on c-BN are shown in Figure 3.13. Deconvolution of (i) shows the B_{1s} and N_{1s} core levels of the hydrogenated sample, as discussed earlier. Open circles indicate the acquired data, full lines the least square curve fitting results.

Core level spectra in (ii) show a Boron Nitride sample with Diazonium linker. From the c-BN and h-BN peak contributions, the quality of this film can be evaluated. The high h-BN contribution in both B_{1s} and N_{1s} indicates that the surface mainly consists of the sp^2 bonded hexagonal phase of Boron Nitride. This observation is supported by a high $\pi \rightarrow \pi^*$ shake-up line in the plasmon region scan of boron and nitrogen. GATR Infrared Spectroscopy revealed, that the cubic content of this film is only 24.3 %. This is reflected in both B_{1s} and N_{1s} core level spectra by a h-BN/c-BN ratio of 0.735 and 0.729, respectively.

Since GATR was not accessible until the last month of this work and the analyzation chamber was broken at this time, the deviating cubic phase volume fractions could not be quantified in time to repeat the functionalization with a better suited sample.

Similar to N_{1s} core level spectra from Fatty Acid linking, N_{1s} in Diazonium linking show a new contribution after linkage at 399.3 eV which can be attributed to the N–C bond [5,36,39]. Since no other N–C bond than that from nitrogen in the BN to the Diazonium linker are present at this time, Diazonium binds to nitrogen at the thin film surface. The C_{1s} core level spectrum also shows a C–N contribution at 286.4 eV [35,40] supporting this observation. The missing B–C contribution at 189.6 eV [36,40,41] from the B_{1s} spectrum indicates, that binding did occur between Diazonium and nitrogen alone.

From the B_{1s} spectrum, a rise in the B–O contribution can be seen which is more pronounced than for the Fatty Acid linker. This may be an effect if the linker, but is more likely correlated to the higher hexagonal phase content in this sample (75.7 %) in comparison to the sample of Fatty Acid linkage (41.6 %).

The C_{1s} core level deconvolution possesses, besides C–C and C–N, a third contribution: COOH at 288.9 eV. This contribution is relevant to estimate the surface coverage of Diazonium on the Boron Nitride surface, since every Diazonium linker contains one carboxyl-group (see Figure 2.5). This leads to a total surface coverage of 4.2×10^{14} Diazonium

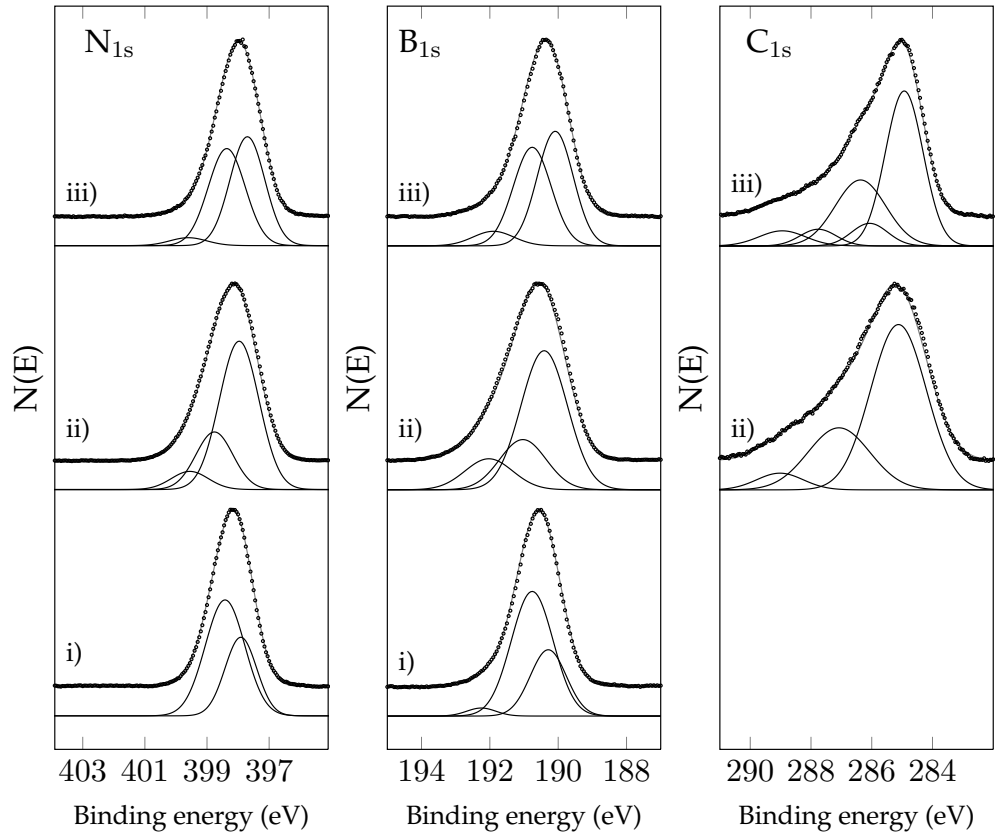

Figure 3.13: XPS core level spectra of Diazonium on c-BN. i) hydrogenated c-BN, ii) Diazonium bound to c-BN, iii) DNA linked to Diazonium on c-BN.
For both N_{1s} and B_{1s} , sp^2 and sp^3 contributions are present. N_{1s} i) and ii) show an N–C contribution. B_{1s} exhibits a B–O contribution. C_{1s} ii) includes COOH and C–N contributions and C_{1s} iii) gives possible peak contributions for C–C, C–N, C=N, C–O and C=O. All spectra are normalized to 100 % intensity.

molecules per cm^2. The N–C contribution from N_{1s} spectrum corresponds to a surface coverage of the same magnitude. This Diazonium linker surface coverage is more than two times as much as the surface coverage of Fatty Acid linker ($1.8 \times 10^{14}\,cm^{-2}$, see section 3.2).

The core level spectra of DNA linked to Diazonium at the c-BN surface are given in Figure 3.13 (iii). The cubic phase content of 48.2 % that was detected from GATR spectra resembles the h-BN/c-BN ratio of 0.52 and 0.51 for B_{1s} and N_{1s}, respectively. It can be noted, that the B–O contribution in the B_{1s} spectra is reduced in comparison to that from Diazonium on BN (ii). Since the samples were not prepared in series, but Diazonium and Diazonium + DNA exist on two independent samples,

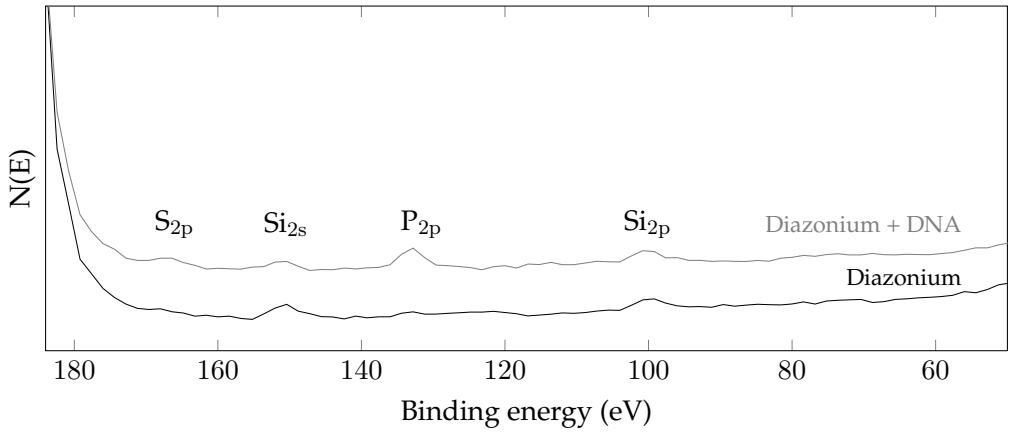

Figure 3.14: XPS spectra of Diazonium linker on c-BN and Diazonium bound to DNA on c-BN. The silicon contamination originates from hydrogenation and contaminated DNA, sulfur from the ALEXA 488 label and phosphor from phosphate groups within the DNA itself.

the B–O contribution did not necessarily diminish. It is more likely that by the higher cubic phase content of (iii), the ability to incorporate oxygen is reduced.

The relative decrease of the N–C contribution in the N_{1s} core level spectrum in contrast to the Diazonium sample on the other hand can not be explained by different quality of samples. Here the addition of DNA to the sample decreases the overall N/C ratio due to the quantity of amine-bonds in comparison to the amount of alkane-bonds in the DNA.

The deconvoluted C_{1s} core level spectrum in Figure 3.13 (iii) gives an estimation of possible peak contributions present in Diazonium and DNA, amongst which are C–C, C–O, C=O, C–N, and C=N. The great variety of bond types makes deconvolution manifold and allows a set of interpretations. For this work, the information gained from the other core level spectra already allows conclusions and controls for these conclusions, so the main focus lies upon them.

To quantify the surface coverage of DNA on the functionalized samples, the enlarged spectral region between 180 eV and 60 eV for both Diazonium and Diazonium and DNA (see Figure 3.14) is being investigated.

Similar to the previously described samples, silicon contaminations are present in both samples. Besides these two Si_{2s} and Si_{2p} peaks, the Diazonium sample contains no other elements in this scan range. On

coupling DNA to the Diazonium, sulfur from the ALEXA 488 label and phosphor from phosphate groups in the DNA emerge in the spectrum. The theoretical ratio of P/S is 4/1, in this sample it is 3.4/1. Regarding the high scan steps of 0.2 eV, the high pass energy of 187 eV and the small intensity of the peaks, this deviation from the theoretical value can be explained with the error in curve fitting and the lack in resolution. A fine scan of this region would improve the signal-to-noise ratio and the resolution.

The ALEXA 488 label contains two sulfate groups and each ssDNA strand is labeled, hence every DNA molecule exhibits the signal of two sulfur atoms in XPS. Knowing this, the surface coverage of DNA can be calculated from the corrected peak area of the S_{2p} peak and leads to a value of 8.6×10^{12} DNA molecules per cm^2.

The Diazonium linked DNA surface coverage is only slightly higher than the surface coverage of Fatty Acid linked DNA ($7.5 \times 10^{12} cm^{-2}$, see section 3.2), although the surface coverage of linker molecules has more than doubled. This indicates, that the maximum surface coverage of 8 base pair DNA including the ALEXA 488 label on c-BN lies within the experimentally maintained range.

Comparing the fluorescent images of Fatty Acid + DNA (Figure 3.9) and Diazonium + DNA (Figure 3.12), a clear difference in color between both positive samples is noticeable. Since the surface coverage is in the same order of magnitude, this difference needs explanation:

Emission light brightness can be adjusted with the confocal microscope. Changing the focus of illuminating light results in differences in emission light. From batch to batch, the laser intensity may vary due to different stages of laser runtime. For objective comparison, the bleached region and its intensity difference to the non bleached region is of interest. For both Fatty Acid and Diazonium this difference is in the same order of magnitude (82 % and 86 % of initial intensity in the bleached region of interest, respectively), stating that bleaching same fluorophores with the same intensity for the same amount of time results in equal bleaching. Thus, the similar surface coverage is represented by similar bleaching and not by the absolute color or brightness of confocal images.

3.4 Direct DNA linking

Direct coupling of DNA to the c-BN surface showed no increased intensity in confocal imaging (see Figure 3.15). Image (a) shows the fluorescence of NH_2-DNA before photo bleach and (b) shows the same region after photo bleach. The positive control of carboxyl-DNA shows no difference in intensity of emitted light. The few bright spots in the images arise from agglomerated DNA that was not washed off from the sample.

Bleaching a rectangular region of interest on both the positive control (COOH-DNA) and negative control (NH_2-DNA) did not reduce the fluorescence which indicates that the green color of the images is not due to fluorescence but to reflection of the illuminating light. It can be seen that photo-bleaching worked well, since DNA-agglomerates lying in the region of interest clearly decrease in intensity (marked by white arrows in the images of Figure 3.15 b) and d).

Neither the positive control nor the negative control DNA did covalently bind to c-BN. Washing with SDS and SSC removed the unbound DNA leaving only few agglomerated DNA spots with their fluorophores for confocal imaging.

The XPS spectra in Figure 3.16 and Figure 3.17 give a possible explanation to this observation. The carboxyl-DNA as positive control contains a significant amount of silicon. Calculations showed, that the silicon in this sample had a surface content of 55.12 % which is more than 1/2 monolayer of silicon at the sample surface. Since COOH can only be coupled by the EDC-protocol to possible NH_2-groups from the surface, and the surface contains boron and nitrogen in equal parts, the carboxyl-

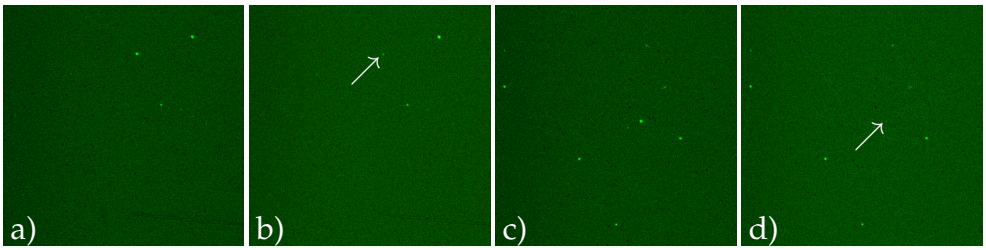

Figure 3.15: a) amine-DNA before photo-bleach, b) amine-DNA after photo-bleach, c) carbxyl-DNA before photo-bleach, d) carboxyl-DNA after photo-bleach. Bleached region is marked by white arrows. No change in the rectangular region of interest indicates missing fluorophores. Bright spots show residual agglomerations of DNA on the surface.

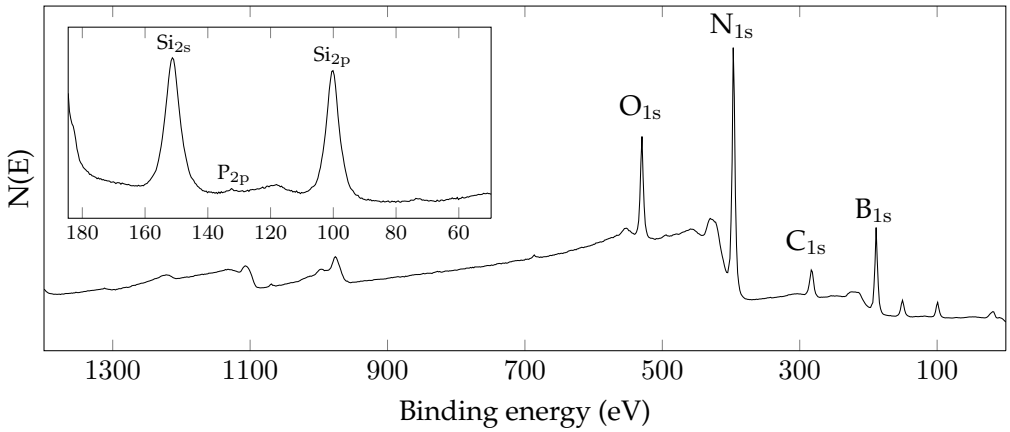

Figure 3.16: XPS spectrum of carboxyl-DNA on c-BN: Positive control for direct linking of DNA to c-BN through the EDC-protocol. High amount of silicon contaminations are present.

groups from DNA strands may only have around 22 % free binding sites to attach to if half of the binding sites are covered with silicon and half of the remaining sites is boron. Fluorescence images showed, that not even these few binding sites served for coupling.

XPS spectra taken from pure amine- and carboxyl-DNA showed, that the Si/C ratio between pure amine-DNA and carboxyl-DNA differs by a factor of 4. This means that the commercially available carboxyl-DNA is contaminated four times as much with silicon than the amine terminated DNA. In the functionalized samples, this factor increased to 5, stating that the silicon contamination in carboxyl-DNA modified samples is five times as much as in amine-DNA modified samples.

The NH_2-DNA as negative control only contains 9.70 % of silicon at the surface, which is less than 1/10 monolayer. This contamination of the negative control can be neglected since the NH_2-DNA will neither bind to NH_2-groups at the sample surface nor bind to the silicon contaminations and cannot be bound through a nucleophilic substitution by the EDC-protocol to boron. The result of the negative control therefore is clear: Amine-DNA does not bind to c-BN surfaces if mediated with the EDC-protocol. The negative control hence shows no binding, as expected.

The positive control on the other hand does not allow a clear statement whether linkage of carboxyl-DNA to c-BN is possible or not. It still needs to be investigated, if carboxyl-DNA binds to c-BN if there is no silicon contamination in the purchased DNA. Only by reducing the amount of

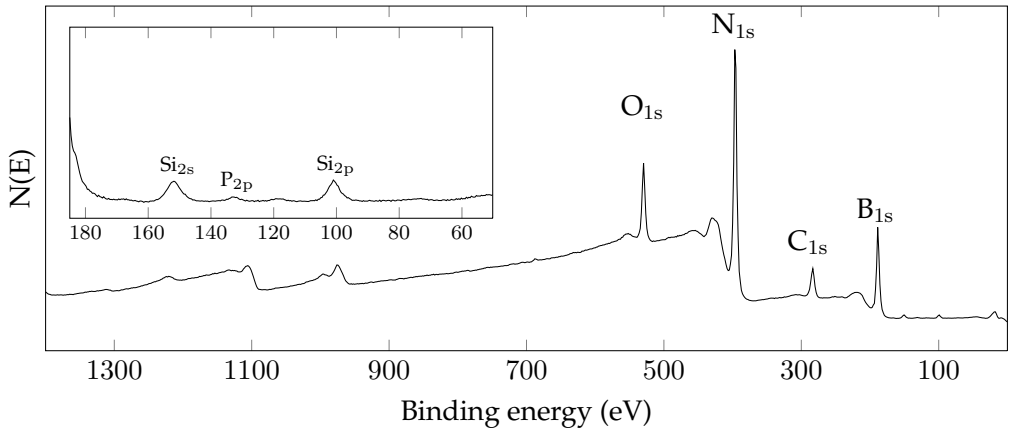

Figure 3.17: XPS spectrum of amine-DNA on c-BN: Negative control for direct linking of DNA to c-BN through the EDC-protocol.

contaminations at the sample surface can give comparable results. The fact that carboxyl-DNA in this work did not bind to the c-BN surface is not necessarily a proof that it is not possible to do so.

In the scope of this study, a more thorough set of experiments to confirm the above mentioned observations was not possible due to problems with both the hydrogenation chamber and the analyzation chamber in the final time period of this work.

4 Conclusion

For this work, cubic Boron Nitride thin films were grown on nanocrystalline diamond. Clean and contamination free NCD thin films on silicon served as substrate for further c-BN growth. Deposition parameters for the growth of c-BN thin films were chosen to create high quality films. XPS, AFM and FTIR analysis showed, that the c-BN thin films covered the NCD film completely, the surface roughness slightly decreased and a cubic phase content of more than 70 % could be achieved using r.f. magnetron sputtering.

Hydrogenation of the c-BN thin films resulted in slightly oxidized boron at the thin film surface with an overall surface content of 15.6 %. Silicon contaminations were brought onto the sample by the hydrogenation process and resulted in 3.2 % silicon at the surface. Carbon contaminations on the thin film arise from the ex situ hydrogenation process, from particles gravitating on the films.

Ion implanted argon in the top layers of the thin film could be removed by the hydrogenation process, the previously reported h-BN like top layers were partly removed by the etching process taking place under hydrogenation.

The Surface Free Energy calculations and the contact angel measurements revealed a hydrophilic character of c-BN and an unstable hydrogenation termination layer of the surface due to a rapid decrease in contact angle in the first 20 min before a stable value of 27° is reached.

Surface Free Energy calculations with different contact angle results for four liquids with known polar and dispersive components revealed a total Surface Free Energy of 60.86 mJ/m^2. Cubic Boron Nitride exhibits a high polar component of 26.73 mJ/m^2 of the Surface Free Energy and a dispersive component of 34.13 mJ/m^2.

Different approaches of functionalization for Boron Nitride thin films were investigated. It could be shown, that functionalization c-BN with linker molecules recently used for diamond functionalization worked well for both Fatty Acid and Diazonium with c-BN as substrate.

Table 4.1: Surface coverages for both Fatty Acid and Diazonium linker. The atomic density of c-BN is 1.68×10^{23} cm^{-3}, its surface density is 3.04×10^{15} cm^{-2}.

	Surface coverage linker	Surface coverage DNA
Fatty Acid	1.8×10^{14} cm^{-2}	7.5×10^{12} cm^{-2}
Diazonium	4.2×10^{14} cm^{-2}	8.6×10^{12} cm^{-2}

Although Diazonium linkage resulted in a surface coverage more than two times higher than for Fatty Acid, the surface coverage of DNA for both approaches lies within the same order of magnitude (see Table 4.1). This confirms the assumption that the maximal DNA surface coverage has been reached by both types of linker molecule. A high deviation in cubic phase content for the samples of Diazonium linkage could only be detected in the last period of this work when a reproduction of the affected samples could not be performed.

Direct coupling of DNA to the c-BN surface did not give evaluable results for binding. The fluorescence images showed only traces of DNA at the sample surface after the normal washing procedure with SDS, indicating that no covalent bond between the c-BN thin film and the carboxyl-DNA could be mediated by the EDC-protocol. Since the purchased carboxyl-DNA contained a significant amount of silicon, it can not be proclaimed with safety that direct coupling of carboxyl-DNA to c-BN with EDC is not possible.

Variations in cubic phase content of the different samples were present in the samples of this work. Deconvolution of the XPS core level scans for B_{1s} and N_{1s} illustrate these deviations in changing c-BN and h-BN peak contributions that are consistent with FTIR and GATR results and in extreme cases with an increased $\pi \rightarrow \pi^*$ shake-up line in the plasmon region of boron and nitrogen.

Difficulties in data comparability emerge from the fact, that the cubic phase content differs from sample to sample. This could be eliminated by using double sided polished wafers to allow fast transmission FTIR as quality check. Deficient quality samples thus could be excluded from further hydrogenation and functionalization. Single sided polished silicon substrates should only serve as thin film platform, if GATR is available for fast analysis.

The use of different samples for analyzation of bare c-BN, hydrogenated c-BN, c-BN functionalized with linker and c-BN functionalized

with DNA should be avoided in further experiments. These deviations in sample quality and contaminations makes comparability and reproducibility challenging.

Different problems have been faced in this work. The quality control and determination of cubic phase content for single side polished silicon substrate was only possible using GATR, since transmission FTIR is not possible due to the high surface roughness of the unpolished side leading to high scattering of the infrared light and thus decreasing the infrared light intensity to undetectable signals. Scratches in the crystal of the GATR device demanded time consuming repair of the equipment abroad and made the control for functionalized samples impossible until few weeks before the closing date of this thesis. Changing to double sided polished silicon wafers as substrate resolved the problem and allowed in house FTIR, nevertheless due to a contaminated hydrogen plasma chamber and a broken analyzation chamber in the final period of this work, this approach could not be completed.

Finally, the silicon contaminated c-BN thin films on NCD substrates with deviating cubic phase content needed to be taken for investigation and analyzation in this work. Reproduction of functionalization on substrates with equal content of cubic phase and contamination free hydrogenation would help support the gained results and to eliminate deviating results due to variations in substrates and thin films.

In conclusion, it can be stated that both Fatty Acid and Diazonium linker served well for functionalization of c-BN thin films. The final DNA surface coverage for both types of linker molecule is in the same order of magnitude.

Due to the long illuminating time of 20 h needed for the coupling of Fatty Acid to c-BN in respect to only 1 h binding time for Diazonium, the Diazonium linker exhibits the advantage of a less time consuming and easier binding procedure.

References

[1] B.R. Eggins. *Chemical Sensors and Biosensors*. Wiley, 2002.

[2] N. Bijnens, V. Vermeeren, M. Daenen, L. Grieten, K. Haenen, S. Wenmackers, O Williams, M. Ameloot, M. vandeVen, L. Michiels, and P. Wagner. Synthetic diamond films as a platform material for label-free protein sensors. *Physica Status Solidi A*, 206:520–526, 2009.

[3] S. Szunerits and R. Boukherroub. Different strategies for functionalization of diamond surfaces. *Solid State Electronics*, 12:1205–1218, 2008.

[4] W.J. Zhang, X.M. Meng, C.Y. Chan, K.M Chan, Y. Wu, I. Bello, and S.T. Lee. Interfacial study of cubic boron nitride films deposited on diamond. *Journal of Physical Chemistry B*, 109(33):16005–16010, 2005.

[5] Y. Zhou, J. Zhi, P. Wang, Y. Chong, Y. Zou, W. Zhang, and S. Lee. Surface functionalization of cubic boron nitride films for biological sensing applications. *Applied Physics Letter*, 92(163105), 2008.

[6] P. Mirkarimi, K. McCarty, and D. Medlin. Review of advances in cubic boron nitride thin film synthesis. *Materials Science and Engineering*, 21:47–100, 1997.

[7] R.H. Wentorf. Cubic form of boron nitride. *Journal of Chemical Physics*, 26(4):956, 1957.

[8] N. Deynek, X.W. Zhang, H.-G. Boyen, P. Ziemann, and F. Banhart. Growth of cubic boron nitride films on Si by ion beam assisted deposition at the high temperatures. *Diamonds and Related Materials*, 13:473–481, 2004.

[9] W. Zhang, Y. Chong, I. Bello, and S. Lee. Nucleation, growth and characterization of cubic boron nitride (cBN) films. *Journal of Physics D: Applied Physics*, 40:6195–6174, 2007.

[10] X.W. Zhang, H.-G. Boyen, P. Ziemann, M. Ozawa, F. Banhart, and M. Schreck. Growth mechanism for epitaxial cubic boron nitride films on diamond substrates by ion beam assisted deposition. *Diamonds and Related Materials*, 13:1144–1148, 2004.

[11] P. Widmayer, H.-G. Boyen, P. Ziemann, P. Reinke, and P. Oelhafen. Electron spectroscopy on boron nitride thin films: Comparison of near-surface to bulk electronic properties. *Physical Review B*, 59(7):5233–5241, 1999.

[12] W. Kern. *Handbook of Semiconductor Wafer Cleaning Technology — Science, Technology, and Applications*. Wiliam Andrew Publishing, 1993.

[13] P. Christiaens, V. Vermeeren, S. Wenmackers, M. Daenen, K. Haenen, M. Nesládek, M. vandeVen, M. Ameloot, L. Michiels, and P. Wagner. EDC-mediated DNA attachment to nanocrystalline CVD diamond films. *Biosensors and Bioelectronics*, 22:170–177, 2006.

[14] T. Knickerbocker, T. Strother, M.P. Schwartz, J.N. Russell, J. Butler, L.M. Smith, and R. J. Hamers. DNA-Modified Diamond Surfaces. *Langmuir*, 19:1938–1942, 2003.

[15] C. Stavis, T. L. Clare, J. E. Butler, A. D. Radadia, R. Carr, H. Zeng, W. P. King, J. A. Carlisle, A. Aksimentiev, R. Bashir, and R. J. Hamers. Surface functionalization of thin-film diamond for highly stable and selective biological interfaces. *PNAS*, 108(3):983–988, 2011.

[16] B.P. Corgier, A. Laurent, P. Perriat, L.J. Blum, and C.A. Marquette. A versatile method for direct and covalent immobilization of DNA and proteins on biochips. *Angewandte Chemie International Edition*, 46:4108–4110, 2007.

[17] J. Pinson and F. Podvoricab. Attachment of organic layers to conductive or semiconductive surfaces by reduction of diazonium salts. *Chemical Society Reviews*, 34:429–439, 2005.

[18] T.-C. Kuo, R. L. McCreery, and G. M. Swain. Electrochemical modification of boron-doped chemical vapor deposited diamond surfaces with covalently bonded monolayers. *Electrochemical and Solid-State Letters*, 2(6):288–290, 1999.

[19] A. Einstein. Über einen die Erzeugung und Verwandlung des Lichtes betreffenden heuristischen Gesichtspunkt. *Annalen der Physik*, 17(132–148), 1905.

[20] D. Briggs and M. P. Seah. *Practical Surface Analysis: Auger and X-Ray Photoelectron Spectroscopy*, volume 1. Wiley, 1996.

[21] C.D. Wagner, W.M Riggs, L.E. Davis, J.F. Moulder, and G.E. Muilenberg. *Handbook of X-Ray Photoelectron Spectroscopy*. Perkin-Elmer, 1997.

[22] C. D. Wagner, L. E. Davis, M. V. Zeller, J. A. Taylor, R. H. Raymond, and L. H. Gale. Empirical atomic sensitivity factors for quantitative analysis by electron spectroscopy for chemical analysis. *Surface and Interface Analysis*, 3(5):211–225, 1981.

[23] S. Geng, A. Zhang, and H. Onishi. Precision thickness measurement of ultra-thin films via XPS. *Materials Science Forum*, 437–438:195–198, 2003.

[24] S. Tanuma, C.J. Powell, and D.R. Penn. Material dependence of electron inelastic mean free paths at low energies. *Journal of Vacuum Science and Technology*, 8, 1990.

[25] C.K. Man. *Synthesis and Characterization of Cubic Boron Nitride*. PhD thesis, City University of Hong Kong, 2004.

[26] H. Yin. *Doping of high quality cubic boron nitride films epitaxially grown in (001) diamonds*. PhD thesis, Universität Ulm, 2007.

[27] Y. Chong. *The study of cubic boron nitride/diamond composite films for sensing and mechanical applications*. PhD thesis, City University of Hong Kong, 2009.

[28] J.F. Watts and J. Wolstenholme. *An introduction to surface analysis by XPS and AES*. Wiley, 2003.

[29] T. Young. An essay on the cohesion of fluids. *Philosophical Transactions of the Royal Society of London*, 95:65–87, 1805.

[30] D.K. Owens and R.C. Wendt. Estimation of the surface free energy of polymers. *Journal of Applied Polymer Sciences*, 13:1741–1747, 1969.

[31] M. Żenkiewicz. Methods for the calculation of surface free energy of solids. *Journal of Achievements in Materials and Manufacturing Engineering*, 24:137–145, 2007.

[32] O. Planišek, A. Trojak, and S. Srčič. The dispersive component of the surface free energy of powders assessed using inverse gas chromatography and contact angle measurements. *International Journal of Pharaceutics*, pages 211–217, 2001.

[33] M.N.R. Ashfold, P.W. May, C.A. Rego, and N.M. Everitt. Thin film diamond by chemical vapour deposition methods. *Chemical Society Reviews*, 25(27):21–30, 1994.

[34] Y.K. Lee and H. Oechsner. On the influence of substrate temperature for cubic boron nitride growth. *Thin Solid Films*, 437:83–88, 2003.

[35] H. Aoki, T. Masuzumi, D. Watanabe, M.K. Mazunder, H. Sota, C. Kimura, and T. Sugino. Influence of oxygen plasma treatment on boron carbon nitride film composition. *Applied Surface Science*, 255:3635–3628, 2009.

[36] Y. Etou, T. Tai, T. Sugiyama, and T. Sugino. Characterization of boron carbon nitride films with a low dielectric constant. *Diamonds and Related Materials*, 11:985–988, 2002.

[37] D. Schild, S. Ulrich, J. Ye, and M. Stüber. Xps investigations of thick, oxygen-containing cubic boron nitride coatings. *Solid State Sciences*, 12:1903–1906, 2010.

[38] N. Rathod. The effects of surface properties of boron nitride on polymer processability. Master's thesis, University of British Columbia, 2003.

[39] A. Perrone, A.P. Caricato, A. Luches, M. Diescu, C. Ghica, V. Sandu, and A. Andrei. Boron carbonitride films deposited by pulsed laser ablation. *Applied Surface Science*, 133:239–242, 1998.

[40] M.A. Mannan, M. Nagano, K. Shigezumi, T. Kida, N. Hirao, and Y. Baba. Characterization of boron carbonitride (BCN) thin films deposited ba radiofrequency and microwave plasma enhanced chemical vapor deposition. *American Journal of Applied Sciences*, 5(6):736–741, 2007.

[41] M.C. Polo, E. Martínez, J. Esteve, and J.L. Andújar. Preparation of B–C–N thin films by r.f. plasma assisted CVD. *Diamonds and Related Materials*, 7:376–379, 1998.

[42] A.F. Azevedo, J.T. Matsushima, F.C. Vicentin, M.R. Baldan, and N.G. Ferreira. Surface characterization of NCD films as a function of sp^2/sp^3 carbon and oxygen content. *Applied Surface Science*, 255:6565–6570, 2009.

Auteursrechtelijke overeenkomst

Ik/wij verlenen het wereldwijde auteursrecht voor de ingediende eindverhandeling:
Cubic Boron Nitride Thin Films as Alternative Platform for Biosensor Applications

Richting: **master in de biomedische wetenschappen-bio-elektronica en nanotechnologie**
Jaar: **2011**

in alle mogelijke mediaformaten, - bestaande en in de toekomst te ontwikkelen - , aan de Universiteit Hasselt.

Niet tegenstaand deze toekenning van het auteursrecht aan de Universiteit Hasselt behoud ik als auteur het recht om de eindverhandeling, - in zijn geheel of gedeeltelijk -, vrij te reproduceren, (her)publiceren of distribueren zonder de toelating te moeten verkrijgen van de Universiteit Hasselt.

Ik bevestig dat de eindverhandeling mijn origineel werk is, en dat ik het recht heb om de rechten te verlenen die in deze overeenkomst worden beschreven. Ik verklaar tevens dat de eindverhandeling, naar mijn weten, het auteursrecht van anderen niet overtreedt.

Ik verklaar tevens dat ik voor het materiaal in de eindverhandeling dat beschermd wordt door het auteursrecht, de nodige toelatingen heb verkregen zodat ik deze ook aan de Universiteit Hasselt kan overdragen en dat dit duidelijk in de tekst en inhoud van de eindverhandeling werd genotificeerd.

Universiteit Hasselt zal mij als auteur(s) van de eindverhandeling identificeren en zal geen wijzigingen aanbrengen aan de eindverhandeling, uitgezonderd deze toegelaten door deze overeenkomst.

Voor akkoord,

Wilbers, Fabian

Datum: **14/06/2011**